Thesis for the Master's Degree
in Chemistry

Leva Momtazi

Synthesis and Characterization of Magnetic Nanocarriers for Cancer Drug Delivery

60 study points

DEPARTMENT OF CHEMISTRY

Faculty of Mathematics
and Natural Sciences
UNIVERSITY OF OSLO

January 2014

Acknowledgment

My first and sincere appreciation goes to my supervisor, Professor Bo Nyström, for his patience, motivation, enthusiasm and immense knowledge. His guidance helped me in the time of research and writing of this thesis. I also would like to express my deep gratitude and respect to my co-supervisor Dr. Shahla Bagherifam whose advice and insight was valuable to me. In addition I would like to thank Dr. Reidar Lund for guiding my research in light scattering field.

My special thanks to Dorna misaghian who did the HPLC measurements and Antje Hofgaard for cross-sectioning the cells. I would like to thank Professor Gunhild Mælandsmo who provided us with breast cancer cell line in the laboratory of the Radium Hospital. I wish to express my warm and sincere thanks to Arash Rayzan for helping me with illustrating the images in this thesis. Moreover, I would like to thank Professor Gareth Griffiths who gave feedback on cell uptake section of the thesis.

I would like to thank my fellow labmates in the group: Sara Bekhradnia, Farinaz Kahnamouei, Golnaz Isapour, Elahe Jafari, Neda Khorshid, for the stimulating discussions, for the sleepless nights we were working together, and for all the fun we have had in the last two years.

Last but not least I would like to thank my family: Maman, Baba, Vahid and Vesal to support me emotionally. My deepest appreciation is expressed to them for their love, understanding, and inspiration.

Leva Momtazi

University of Oslo

January 2014

Abstract

A targetable nanocarrier consisting of a superpara-magnetic iron oxide (SPIO) core and a biodegradable and biocompatible polymer shell with the potential application in drug delivery system was prepared. The biodegradable and biocompatible poly (sebacic anhydride)-*block*-methylether-poly (ethylene glycol) (PSA-mPEG) was synthesized with poly condensation method to be used as the polymer shell for encapsulation of SPIO nanoparticles (SPIO-NPs). The synthesized block copolymer was charachterized by ^{1}HNMR, FTIR and GPC. The change in chemical structure and molecular weight of the polymer in PBS at 37°C was studied by FTIR and GPC.

The magnetic nanocarriers were synthesized by nanoprecipitation method and morphology of these nanocarriers was studied by transmission electron microscopy (TEM). The size and iron oxide content of the nanocarriers were studied by dynamic light scattering (DLS) and inductively coupled plasma spectroscopy (ICP-MS) respectively, to find an optimal carrier system for delivering therapeutic agents to the tumor site.

The zeta potential measurement was conducted on nanoparticles in both deionized water and phosphate buffer saline (PBS) to evaluate the surface charge of the particles in these mediums. The hydrodynamic radius (R_h) of the SPIO loaded polymeric nanoparticles (SPIO-PNP) was measured over 30 days .The R_h did not change considerably so it can be concluded that the particles were stable in this time period.

The cytotoxicity of SPIO-PNPs, SPIO-NPs and blank polymeric nanoparticles were investigated on MDA-MB-231 breast cancer cell line. The cell viability was high (> 85%) for all three samples meaning that they did not induce toxicity.

The internalization of SPIO-PNP in MDA-MB-231 cell line was confirmed by TEM. To make sure that the particles are confined within cells, the nanoparticle treated cells were fixed by glutaraldehyde and later cross sectioned.

Contents

List of figures

List of tables

List of symbols and abbreviations

A_f	Amplitude for fast relaxation time in DLS
A_s	Amplitude for slow relaxation time in DLS
β	width of the distributions of relaxation time
CMC	Critical Micelle Concentration
$\mathbf{D_f}$	Apparent diffusion coefficient for fast mode
DCM	Dichloromethane
DLS	Dynamic Light Scattering
DOX	Doxorubicin
ε	Dielectric constant
EPR	Enhanced Permeability and Retention
η	Viscosity
$\mathbf{g^1(q,t)}$	First order electric field autocorrelation in DLS
$\mathbf{g^2(q,t)}$	Intensity autocorrelation function in DLS
GPC	Gel Permeation Chromatography
Γ	Gamma function
HPLC	High-Performance Liquid Chromatography
ICP-MS	Inductively Coupled Plasma Mass spectroscopy
$\mathbf{k_B}$	Boltzmann constant
λ	Wavelength
mPEG	Methyl ether poly(ethylene glycol)
MTS	[3-(4,5-dimethylthiazol-2-yl)-5-(3-carboxymethoxyphenyl)-2-(4-sulfophenyl)-2H-tetrazolium]
$\mathbf{M_n}$	Number average molecular weight
$\mathbf{M_w}$	Weight average molecular weight
nm	Nanometer
NP	Nanoparticle
PBS	Phosphate Buffer Saline
PCL-PEG	Poly (ε-caprolactone)- poly(ethylene glycol)
PEG	Poly (ethylene glycol)
PLGA	Poly (lactic-co-glycolic acid)
PLGA-PEG	Poly (lactide-co-glycolide)-poly(ethylene glycol)
PNP	Polymeric nanoparticles
PSA	poly (sebacic anhydride)
PSA-mPEG	Poly (Sebacic anhydride)-*block*-methyl ether poly (ethylene glycol) (PSA-mPEG)
PTX	Paclitaxel
PVA	Polyvinyl alcohol
q	Scattering wave vector
$\mathbf{R_h}$	Hydrodynamic radius

RES	Reticulo-Endothelial System
SA	Sebacic acid
SPIO-NP	Superpara-magnetic iron oxide nanoparticle
SPIO-PNP	Superpara-magnetic iron oxide loaded in polymeric nanoparticles
τ_f	Relaxation time for the fast process in DLS
τ_{se}	Relaxation time for the slow process in DLS
θ	Scattering angle
T	Absolute temperature
TEM	Transmission Electron Microscopy
THF	Tetrahydrofurane
ξ	Zeta potential

1. Introduction

The absence of specificity of drugs for tumor cells is a major problem of conventional chemotherapy in cancer treatment. In order to probe sufficient concentration at the tumor, large doses of drug need to be administrated causing the same cytotoxicity in both cancerous and healthy cells. To avoid damage to the healthy tissue, the administrated dose is usually less than optimal. The ideal treatment would provide enough therapeutic agents to eliminate all the cancer cells while leaving the healthy tissue intact. Drug delivery systems are a promising field of interest for tackling these challenges, and can be defined as the process of releasing a bioactive agents at a specific rate and a specific site [1-4].

1.2. Nanotechnology for drug-delivery

By applying nanotechnology in drug delivery, small molecular weight drugs and also macromolecules such as protein, peptide or genes are delivered to the tissue of interest. Therapeutic agents are incorporated in biocompatible nanocomposites such as nanoparticles, nanocapsules and micellar systems in submicron size, and can provide targeted delivery of the drug to sustain drug effect in the target tissue and to protect the therapeutic agent from enzymatic degradation[5].

Among the different types of nanoparticles, superpara-magnetic iron oxide (SPIO) nanoparticles (NPs) are considered to be promising candidates in cancer therapy applications, as carriers in targeted drug delivery systems. Targeting these magnetic carriers by applying magnetic field can eliminate the complications caused by conventional cancer treatment, where the body is flushed by the drug[6].

1.2.1. Nanoparticulate drug delivery systems formed by amphiphilic block copolymers

Block copolymers with amphiphilic characteristics are macromolecules having a large

solubility difference between hydrophobic and hydrophilic segments with opposite affinities for an aqueous solvent. Block copolymers are at the center of attention in drug delivery systems because of their ability to form various types of nanoparticles. For drug delivery purposes, biocompatible and biodegradable polymers like polyesters, poly (amino acids) or poly anhydride can be used. These hydrophobic blocks are covalently bonded to biocompatible hydrophilic blocks like polyethylene glycol (PEG). Amphiphilic copolymers have the ability to form nanoparticles with different structures namely: micelles, nanospheres, nanocapsules and polymerases (Figure 1-1) [7].

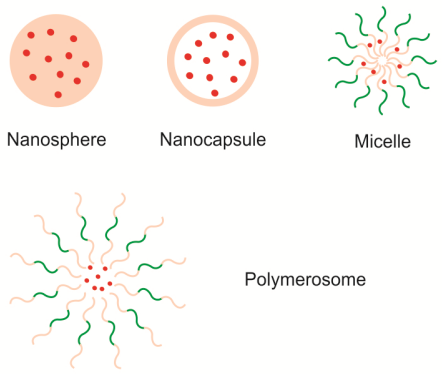

Figure 1-1: General architecture of Nanoparticulate drug delivery systems formed by amphiphilic block copolymers

1.2.1.1. Micelles

Micellar self-association takes place above the critical micelle concentration (CMC) in a dilute solution of block copolymer in a specific solvent and at fixed temperature. In an aqueous solution, this phenomenon occurs because the amphiphilic copolymer orients itself in a way that hydrophobic blocks try to avoid the aqueous medium and achieve the minimum free energy level. Micellization of block copolymers is strongly dependent on temperature; therefore, for every concentration, a critical micelle concentration is specified. The self-assembling process of polymer segments may generate a core-sell structure, in which the inner core is composed of hydrophobic segments. This architecture provides the space for solubilization of hydrophobic pharmaceutical agents; the micelle diameter ranges usually from 10 to 100 nm. Micelles are categorized as association or amphiphilic colloids but they

are not considered to be solid particles [7, 8].

1.2.2. Nanospheres

Nanospheres are polymeric matrix systems in which a therapeutic agent is entrapped, encapsulated, absorbed or chemically bounded. In comparison with micelles, nanospheres usually exhibit broader size distribution and they are larger in size. Their diameter is often between 100 to 200 nm. Nanospheres, in contrast to micelles, are classified as solid colloidal particles. Emulsification and nanoprecipitation are the two most important methods of nanosphere preparation. The latter involves dissolution of the block copolymer in an organic water miscible solvent followed by dispersion in aqueous media in presence or absence of surfactant. The water miscible solvent diffuses out in water; and as a consequence, the polymeric particle is formed [7].

1.2.3. Nanocapsules and polymersomes

Nanocapsules are composed of a liquid or semi-liquid core surrounded by a solid material shell. A therapeutic agent can be confined to a reservoir or within a cavity surrounded by a polymer membrane or coating. Nanocapsules have an oil core with the ability to load a high amount of hydrophobic pharmaceutical agent[9]. For nanocapsule formation, the drug is first dissolved in a water-miscible organic solvent. An oil miscible with solvent but immiscible with mixture is added to this solution which is further dispersed in an aqueous media. Consequently, the solvent diffuses into the water and the nanocapsules are formed by aggregation of the polymer around the oil droplet [7, 10].

Alternatively, polymersomes have the same architecture as nanocapsules but in contrast to nanocapsules, the core of vesicle is composed of an aqueous phase with the ability to encapsulate water-soluble drugs [7, 11].

1.3. Targeting the tumor site

After intravenous administration, anti-cancer therapeutic agents are generally cleared from blood circulation rapidly and only a small fraction reaches the tumor site. Besides, reaching the tumor site does not guarantee a strong therapeutic effect because the drug may be cleared from the tumor too rapidly and may not be exposed to the tumor long enough. Another limitation is the physicochemical properties of the drug which makes entering the target cell difficult. In order to suppress these problems, targetable drug delivery systems have been developed. These systems utilize phenotypic properties of the diseased cells to concentrate drug at the target cells. Consequently, the drug is targeted to the tumor site and drug level in the tumor is enhanced [12].

1.3.1. Active targeting

Tumor cells express many molecules on their surface in comparison with normal cells. These molecules can be detected by antibodies. Active targeting displays this characteristic of cancer cells to target the drugs to the tumor site. Active targeting, which is also known as ligand targeting, involves binding of ligands to the surface of drug carriers. These ligands, would then, bind to the molecules expressed on the cancer cells (Figure 1-2)[13]. Folic acid is one the most attractive molecules for targeting cancer cells. Primarily, because the folic acid receptor is overexpressed in many human cancer cells including ovary, brain, kidney, brain, myeloid and lung, and also, because of its high binding affinity, low immunogenicity, ease of modification, small size, stability during storage as well as its low cost [14].

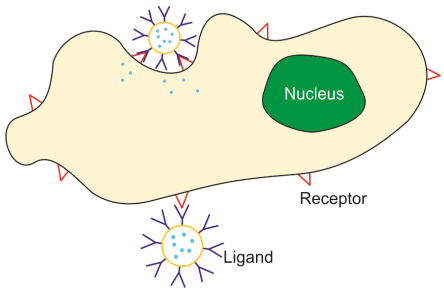

Figure 1-2 : ligand coated nanoparticles for active targeting of cancer cells

1.3.2. Passive targeting

Passive targeting uses the enhanced permeability and retention effect (EPR) as one of the approaches to target nanoparticles to the tumor site. EPR is the result of the combination of leaky vascular and poor lymphatic drainage of a solid tumor. These leaky vessels allow the passage of drug carriers ranging from 10 to 500 nm in size depending on the tumor type and its location in the body. This preferential distribution to the tumor site facilities the eventual release of pharmaceutical agent from the carrier system (Figure 1-3). Particles with an appropriate size must have properties to provide a long circulation time. Longer circulation times can be achieved by surface modification of nanoparticles with polymers with hydrophilic nature such as polyethylene glycol (PEG). There are more aspects to the EPR effect than initially defined, which can give a better understanding of sophisticated processes in cancerous tissues[15].

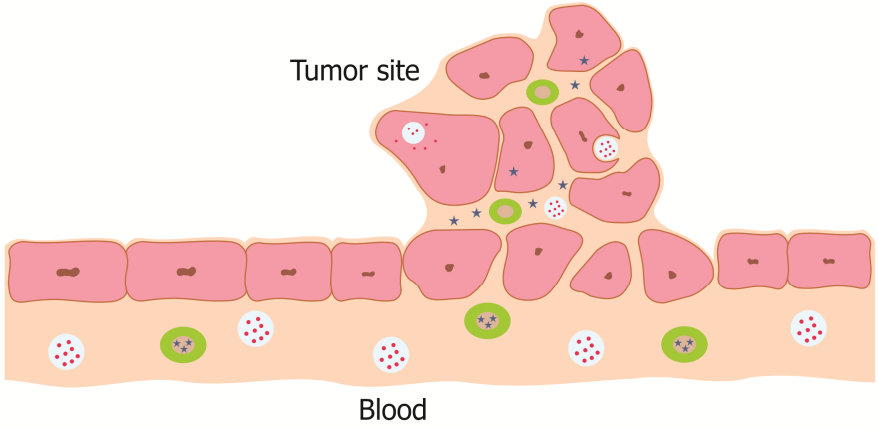

Figure 1-3: accumulation of nanoparticles in tumor cells via EPR effect

1.3.2.1. EPR fundamentals

In a solid tumor, blood vessels are irregular. The reason for this deficiency is that when a solid tumor reaches a certain size, the normal vasculature in its vicinity is not able to provide all the required oxygen supply for the tumor's proliferation. When cells start to die,

they produce growth factors that trigger the budding of new blood vessels from surrounding capillaries. This leads to the rapid formation of new irregular blood vessels in discourteous epithelium which lacks basal membrane of a normal tissue [16, 17].

The enhanced retention component of the EPR effect can be described as follows: in healthy tissues, the extracellular fluid is continuously drained to the lymphatic vessels. This continuous draining, the renewal of interstitial fluid and the recycling of extravasated solutes push the colloids back into circulation, whereas in tumors, the deficiency in lymphatic function and the minimal uptake of interstitial fluid inhibit the return of colloids to the blood stream by convective force. Therefore, nanoparticles that have reached the perivascular site accumulate in tumor [16, 18].

1.3.2.2. Long circulating nanoparticles

PEGylation provides hydrogen bonding between water molecules and the ether oxygens of PEG. The tightly bound water molecules around PEG chains form a hydrated layer around the particle; this minimizes the interactions between nanoparticles and plasma protein [19] which prevents opsonization of the particles by the reticulo-endothelial system (RES). PEG masks the surface of nanoparticles by reducing protein and plasma adsorption to the nanoparticle, inhibiting recognition of PEGylated nanoparticles as foreign objects in the blood stream so the particles can circulate for a longer time. Longer circulation allows the particles to be targeted to the cancerous cells by active or passive targeting. PEGylation can be achieved by several approaches including adsorption of PEG-containing polymers on the surface of nanoparticle, direct conjugation of PEG to the nanoparticles or by using block copolymers, which have PEG in their backbone for forming the nanoparticle [15, 19].

1.3.3. Magnetic particle in biomedicine

Superpara-magnetic iron oxide nanoparticles (SPIO-NPs) are composed of iron oxide cores with the property to be targeted to the desired area through applying an external

magnetic field. Strong permanent magnets like neodymium iron boron (Nd-Fe-B) are widely used for this purpose. Particles with super paramagnetic characteristics have a diameter below ~ $30 - 40\ nm$ which means that once the magnetic field is removed, they do not show any magnetization properties. This feature is very important in clinical applications, because if the particles do not lose their magnetic properties after removing the magnetic field, they tend to aggregate and can be easily recognized by macrophages [6, 20]. Moreover, SIPO-NPs are considered to be benign to the body mainly because under acidic condition, iron oxide is dissolved in the body and forms Fe^{3+}. This increased number of ferric ions adds up to natural ion storage in the body which is 3-5 grams for an adult human [21]. The targetability, together with benignity to the body are two main reasons making SPIO-NPs increasingly attractive in biomedical applications. SPIO-NPs have provided promising features in cancer research as carriers in targeted drug delivery systems, tumor imaging, cancer hyperthermia therapy and other techniques [22].

During the past decades, magnetic nanoparticles and microparticles have been developed to retain drug-loaded particles from blood circulation and deliver it to a specific site *in vivo.* This reduces the distribution of cytotoxic drug leading to a decrease in side effects. The localized targeting of the drug also reduces the required dosage[23]. This drug delivery technique can be used in the case of solid tumors close to the surface of the body because the strength of magnetic field decreases with distance [20].

Magnetic nanoparticles can couple with other targeting strategies for more efficient outcome. Magnetic nanoparticles can passively accumulate in many tumor tissues via the EPR effect owing to their nanosize. Moreover, tumor-selective ligands can be attached to the surface of magnetic nanoparticles to specifically bind to moieties that are over-expressed on the tumor cells. This facilitates active targeting of magnetic particles [24].

1.4. Magnetic drug delivery

Magnetic drug delivery conceptualizes targeting therapeutic agents by either attaching the drug to the surface of magnetic nanoparticle or encapsulating the drug within a

nanocomposite mixture of a polymer and magnetic nanoparticle. The approach of interest in this study lies in the encapsulation of cytotoxic drug along with magnetic nanoparticles inside a polymer matrix (Figure 1-4). Also, the presence of polymer provides a site for anchoring therapeutic drugs or DNA for targeted gene deliver [25].

The large surface area of SPIO-NPs provides the possibility of enhanced covalent attachment of various receptors, antibodies and ligands to bind to specific targets and to release the drug with an appropriate dose [6]. In a recent research, R11 peptides were conjugated to poly (*N*-isopropylacrylamide-acrylamide-allylamine) nanoparticles with iron oxide core for active targeting of drugs for prostate cancer therapy [26].

Once the drug has been incorporated into the nanoparticles and placed *in vivo,* these magnetic nanocomposites are retained at the target site using high-field rare earth magnet [25]. In order to direct the magnetic drug carrier successfully at the target site, the external magnetic force should suppress the blood flow pressure in arteries and capillaries [20]. After concentrating at target, the drug is released by either changing the physiological condition such as pH or temperature or by enzymatic activity [23].

Biodegradable polymer shell carries the drug by either adsorption or entrapment. The incorporation of therapeutic agent and SIPO-NPs in to the polymer shell can be achieved by several techniques such as nano/micro emulsion method, nanoprecipitation method and micelle formation. Self-assembly and nanoparticle formation of amphiphilic block copolymers are promising routes in the formation of multifunctional nanoparticles for imaging and drug delivery applications. In order to enhance the targeting efficiency, the polymer coating can be further functionalized with molecules such as biotin or avidin, which are attach points for targeting antibodies to the carrier complex [23, 27].

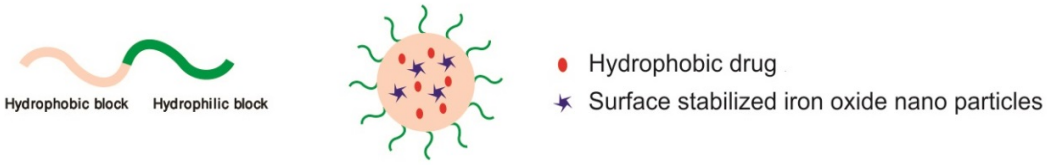

Figure 1-4: encapsulation of hydrophobic drug along with iron oxide nanoparticles inside a polymer matrix

1.4.1. Colloidally stabilized SPIO particles for polymeric drug delivery systems

SIPO-NPs tend to agglomerate due to their large surface area to volume ratio and strong dipole-dipole attraction in both magnetic field and biological medium. This leads to heterogeneous size distribution and rapid clearance from blood stream. To overcome these complications and form a homogenous solution, SIPO-NPs are coated with suitable molecules or polymers. This homogenous solution is called ferrofluid. Steric and electrostatic repulsive forces provided by these agents stabilize the particles in the suspension [28]. The molecules used for stabilizing the SIPO-NPs should be biocompatible and biodegradable idyllically. However, surfactants such as oleic acid, lauric acid and alkane sulphonic acids are the most commonly used molecules. Dimension and surface charge of the particle are other important factors in the stability of SPIO-NPs. Particle size should be sufficiently small so that sedimentation by gravity can be avoided. High surface charge provides dispersion stability due to electrostatic interaction [23].

The nature of functional groups on the surface of SPIO-NPs mostly determines the surface charge of the particle. The surface charge can be measured quantitatively as an electrical potential in the interfacial double-layer on the surface of nanoparticles in suspension. A high zeta potential value, either negative or positive, indicates that the SPIO-PNs are stable in dispersion due to the electrostatic interactions [23].

1.4.2. SPIO-NP synthesis

The most common method for SPIO-NP synthesis is the co-precipitation method which involves addition of base to aqueous solution of ferrous (Fe^{2+}) and ferric (Fe^{3+}) in a 1:2

stoichiometry. The result is a black precipitate of spherical magnetite nanoparticles with uniform size. The size and shape of nanoparticles can be tailored by choosing the appropriate type of salts (e.g. chlorides, sulphates, nitrates, perchlorates, etc.), adjusting Fe^{2+} and Fe^{3+} ratio and controlling pH and ionic strength of media. It should be noted that the reaction needs an oxygen-free environment; otherwise, the magnetite can be further oxidized to ferric hydroxide [29]. The synthesis can be conducted in the presence of some surface-complexing agents, which can provide colloidal stability or biocompatibility. Dextran, Oleic acid and polyethylene glycol (PEG) are among these several SPIO-complexing agents [30].

Recently, the microemulsion technique has been adapted to synthesize-NPs. This technique has the ability to control the size and shape of the particles more preciously. Water in oil is a more common microemulsion technique for SPIO-NP synthesis. In this method, iron salts aqueous nanodroplets are enclosed within surfactant layer and dispersed in an organic phase to form reverse micelle. Adding alkaline nanodroplets to this, results in the formation of SPIO-NPs within the micelles [30, 31].

1.4.3. Applicable polymers in drug delivery systems

Designing polymeric drug delivery systems requires a through consideration of polymer's biocompatibility and biodegradability. Until now, there has been no precise definition or accurate method of determining the biocompatibility due to the intricate nature of interaction between materials and biological systems. In spite of that, a criterion such as acceptance by a living organism can be applied to evaluate biocompatibility. By this definition, in a biocompatible response, toxicity as well as inflammatory, possible immune response and protein adsorption should be reduced to the smallest possible amount. In a biodegradable polymer system, degradation products of a polymer do not evoke immune or toxic response [32].

There are two classes of biodegradable polymers based on their degradation mechanism; hydrolytically degradable polymers and enzymatically degradable polymers.

Most of the naturally occurring polymers undergo enzymatic degradation while polymers with labile chemical bond in their backbone are subjected to hydrolytic degradation. Functional groups such as esters, orthoesters, anhydrides, ureas, etc. may undergo hydrolysis. There are two general mechanisms for synthesizing hydrolytically sensitive polymers for biomedical applications; step (condensation) polymerization and chain (addition) including ring opening polymerization. Condensation mechanism is used to synthesize different hydrolytically sensitive polymer classes, such as polyanhydrides, poly (ortho esters) and poly urethanes [33].

Several biodegradable polymer systems have been pre-clinically investigated during the past decades for localized chemotherapy. These systems include both naturally occurring and synthetic polymers such as polysaccharides (chitosan, alginate and hyaluronan), protein-based polymers (collagen, gelatin and albumin), polyesters and polyanhydrides. Among these different classes of biodegradable polymeric drug carrier systems, only a few polymer-based formulations have reached clinical testing. Poly (lactic-co-glycolic acid) (PLGA) based localized injectable delivery system and implantable polyanhydride copolymer systems for brain cancer treatment are among these clinically tested systems [34-36].

1.4.3.1. Natural polymers

Natural polymers are promising for localized chemotherapeutic delivery systems since they have great biocompatibility and the degradation products are non-toxic and non-immunogenic. However, some complications associated with their purification, immunogenicity and the possible disease transformation from their source organism to humans exist [34].

1.4.3.2. Polyesters

Polyesters are the earliest and most extensively investigated class of biodegradable polymers. Depending on monomer unit, polyesters can be synthesized from various monomers via ring opening and polycondensation polymerization [33]. Among this class of polymers, poly (lactic acid-co glycolic acid) (PLGA) is the most investigated polymer. PLGA has

been used broadly for designing different localized delivery systems such as microparticles and implants. Despite the fact that polyesters' acidic degradation products can lead to local irritation and instability of the drug being delivered, polyester-based drug delivery systems such as PLGA are considered biocompatible and biodegradable [34].

1.4.3.3. Polyanhydrides

Polyanhydrides undergo hydrolytic degradation due to the highly sensitive aliphatic anhydride bond in their backbone. The hydrophobic nature of the polymer, combined with hydrolytically labile backbone, prevents water penetration to polymer matrix, leading to surface erosion of the polymer. This hydrolytic instability, together with surface-eroding characteristic, makes this class of polymers attractive for controlled drug delivery systems. The important characteristic of polyanhydrides is that in contrast to polyesters, they degrade to products which are not cytotoxic or inflammatory. This material was approved by US FDA as a drug delivery carrier in 1966 following extensive in vitro and in vitro drug release and biocompatibility evaluations [33, 34, 37, 38].

Both homo- and co-polyanhydrides with different properties have been synthesized by melt condensation method. The copolymerization of aliphatic polyanhydride like poly (sebacic anhydride) (PSA) with hydrophobic aromatic polymer residues have been investigated to design polymeric systems with controllable degradation rate [33].

1.4.4. Methods for designing magnetic drug carriers

Encapsulating drug molecules along with SPIO-NPs within the polymer coating envelope can be obtained using different methods. Gomez-Lopera et al. described a double-emulsion method for preparing colloidal particles with magnetic core and a biodegradable poly (DL-lactide) polymer shell. The technique includes formation of water in oil emulsion of an aqueous solution of a hydrophilic drug and/or an aqueous suspension of magnetic particles dispersed in an organic solution of polymer. This emulsion is used to prepare the second emulsion in an aqueous surfactant solution. The resultant colloidal particles were both responding to magnetic field and useful as drug delivery system [39].

In a more recent research, an emulsion-diffusion-evaporation technique was used to render nanocarriers loaded with SPIO-NPs and doxorubicin (SPIO/DOX-NP) and nanoparticles loaded with SPIO-NPs and paclitaxel (SPIO/PTX-NP). The SPIO-NPs were surface-modified with oleic acid and dispersed in dichloromethane (DCM) and the three polymers used for the encapsulation of drugs and SPIO were: PLGA, PLGA-PEG, and PCL-PEG. The organic solution contained polymer, SPIO-NPs and the drug. This solution was emulsified by adding the organic phase to an aqueous solution containing a surfactant followed by sonication. The mixture was then added drop-wise and under magnetic stirring to another aqueous phase contacting surfactant and stirred overnight letting the organic solvent evaporates (Figure 1-5)[40].

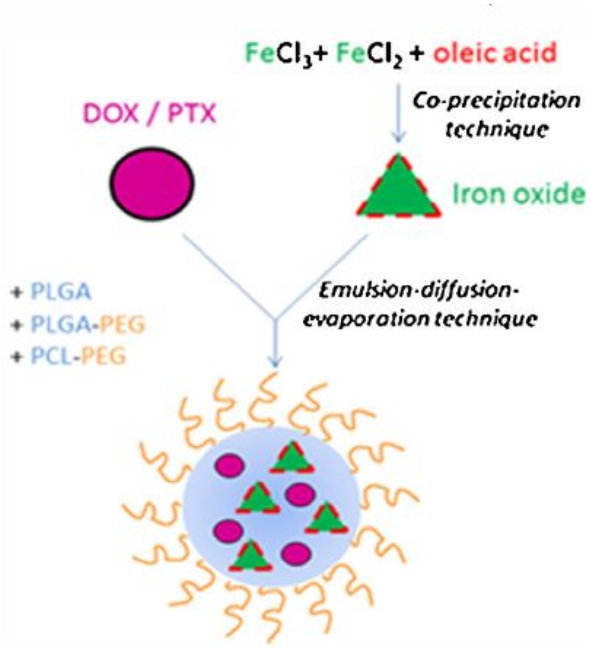

Figure 1-5: nanocarriers loaded with SPIO-NPs and drug [40]

In a different research, Filippousi et al. used the nanoprecipitation method to load taxol and SPIO-NPs within a polymer matrix. Methoxy poly (ethylene glycol)-poly (propylene succinate)-methoxy poly (ethylene glycol) (mPEG-PPSU-mPEG) and taxol were dissolved in tetrahydrofurane (THF) and the SPIO-NPs were dispersed in THF by sonication. By diffusion of this solution into the aqueous phase, multifunctional nanoparticles were formed [41].

1.5. Considerations for designing polymeric magnetic drug delivery systems

When SPIO-NPs are used as drug carriers, size, morphology and charge of the carrier system should be closely investigated. These parameters determine the behavior of drug-loaded nanoparticles in the blood stream and affect blood circulation time as well as bioavailability of the particles in the body. Additionally, magnetic properties and internalization of the particles depend on the size of particles. Particles with a size over 200 nm are concentrated in spleen and, consequently, removed by phagocyte system whereas particles smaller than 10 nm in diameter by renal clearance [29].

1.6. Experimental techniques

This chapter has a closer look on the experimental techniques used to characterize the multifunctional particle with a SIPO-NP core and a biodegradable polymer shell and introduce the biodegradable polymer used for encapsulation of SPIO core.

1.6.1. Introducing Poly (Sebacic anhydride)-*block*-methyl ether poly (ethylene glycol) (PSA-mPEG)

As mentioned in the introduction section, poly anhydrides including poly (sebacic anhydride) provide a controlled drug delivery system for pharmaceutical agents by surface erosion besides polyanhydrides and their degradation products are highly biocompatible.[42]

Due to these important characteristics, (PSA-mPEG) was chosen as the biodegradable polymer shell for encapsulating SIPO-NPs. The block-copolymer was synthesized via melt-condensation method using sebacic anhydride pre-polymer and commercial poly (ethylene glycol) methylene ether (mPEG). The introduction of PEG in copolymer formula adjusts the release rate and hydrophilic properties of the drug delivery system. The chemical structure of the copolymer is depicted below Figure 1-6[42].

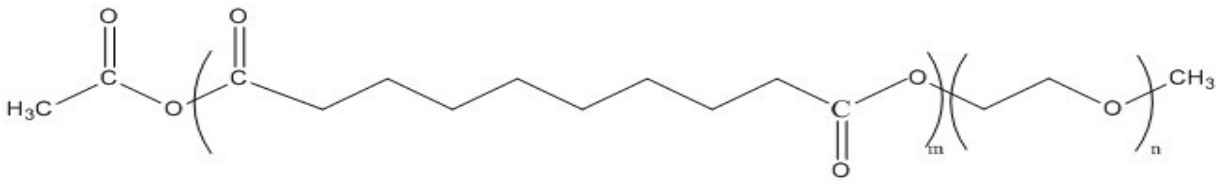

Figure 1-6: chemical structure of PSA-mPEG

1.6.2. Nanoparticle characterization

The focus of this study is on the characterization of these multifunctional nanocarriers rendered by incorporation of SIPO-NPs into a biodegradable polymer shell. Size, morphology, stability, and iron oxide content of these nanocarriers were studied with appropriate experimental techniques. Methods used to study these features are: dynamic light scattering (DLS), zeta potential, transmission electron microscopy (TEM), inductively coupled plasma mass spectroscopy (ICP-MS) and high-performance liquid chromatography (HPLC). Here we discuss the theory and background of zeta potential and dynamic light scattering measurement more closely.

1.6.2.1. Zeta potential

Zeta potential gives an indication about the potential stability of a colloidal system. A large negative or positive potential ($> \pm 30$) results in electrostatic repulsion between the particles, which leads to a greater stability of the particles. By definition, zeta potential of a colloidal system is the potential at the edge of the electrical double layer and it represents the effective surface charge of the particles. In ionic solutions, charged particles have a layer of ions, strongly bound to their surface. A second layer comprise of loosely associated ions diffuses around the first layer. These two layers are known as electrical double layer. When particles move this double layer, the shell is also moved along with the particle [43, 44].

In a zeta potential measurement, the electrophoretic mobility of nanoparticles is determined upon applying an electrical field. Electrophoretic mobility of a particle is the

velocity by which nanoparticles move in a solution. The zeta potential can be determined by equation 1:

$$\xi = \frac{4\pi\eta\mu}{\varepsilon E} \qquad 1$$

Where ξ is the zeta potential (mV), η is the viscosity of the dispersion medium (P), μ is the migration velocity (cm/s), ε is the dielectric constant of the dispersion medium, and E is the potential gradient (Voltage applied/distance between electrodes) [45].

1.6.2.2. Dynamic light scattering (DLS)

DLS determines time-dependent properties such as diffusion coefficient, hydrodynamic radius and its distribution by dynamic changes of scattered light intensity. This random fluctuation in scattered light intensity is due to the Brownian motion of molecules in the solution which is caused by constructive or sometimes instructive light scattered from the molecules in the solution. Detecting these time-dependent fluctuations gives the possibility to explore the relaxation of concentration fluctuations through equilibrium at length scale of q^{-1}.

$$q = \frac{4\pi.n_s}{\lambda}\sin(\frac{\theta}{2}) \quad 2$$

Here q is the wave vector, n_s is the refractive index of the solution, λ is the wavelength of scattering light in a vacuum and θ is the scattering angle. If the scattered field obeys Gaussian statistics, the experimentally obtained normalized intensity autocorrelation function $g^2(q,t)$ is directly related to the first order electric field autocorrelation function $g^1(q,t)$ by the Sigert equation:

$$g^2(q,t) = 1 + B|g^1(q,t)|^2 \quad 3$$

B (≤1) is an empirical factor. The correlation function has been described by a single exponential followed by the stretched exponential at longer times.

$$g^1(q,t) = A_f exp\left[-t/\tau_f\right] + A_s exp\left[-(t/\tau_{se})^{\beta}\right] \quad 4$$

$$A_f + A_s = 1 \qquad 5$$

A_f is the amplitude of the fast mode and A_s is the amplitude of the slow mode. τ_f and τ_{se} are the fast relaxation time and the effective slow relaxation time, respectively. β ($0 < \beta \leq 1$) is the measure of the width of the distributions of relaxation times. The slow relaxation time is calculated by the following equation:

$$\tau_s \equiv \int_0^\infty exp\left[-\left(t/\tau_{se}\right)^{\beta}\right]dt = \left(t/\tau_{se}\right)\Gamma\left(1/\beta\right) \qquad 6$$

Where Γ is the gamma function.

When the fast and slow relaxation modes are diffusive (q^2 dependent):

$$D_f = 1/\tau_f \; q^2 \qquad 7$$

The apparent hydrodynamic radii R_h can be calculated by using Stokes-Einstein equation:

$$R_h = \frac{k_B T}{6\pi\eta D} \qquad 8$$

k_B is the Boltzmann constant, T is the absolute temperature and η is the solvent viscosity [46].

2. Experimental

2.1. Pre-polymer synthesis

Sebacic acid (20.0g) was refluxed with acetic anhydride (200 ml) at 140 °C for 45 minutes under nitrogen atmosphere. Acetic acid and unreacted acetic anhydride were then removed by rotary evaporator at 60°C. The resulting oligomers were recrystallized overnight at 0 °C from dry toluene. The crystals were subsequently added to 200 ml extraction solvent (1:1 dry petroleum ether/di ethyl ether) to extract traces of acetic anhydride and toluene. The purified pre-polymer was dried overnight in vacuum at room temperature (88.5% yield) [47].

2.2. Block copolymer synthesis

Sebacic anhydride pre-polymer (PSA) (4.0g) and poly (ethylene glycol) monomethyl ether (mPEG) (3.0 g) (M_w=2000) were placed in a flask at 180 °C, in vacuum for 2 hours to perform melt-condensation. The raw product was dissolved in 40 ml dry chloroform and precipitated afterwards in 200 ml anhydrous diethyl ether. The purified PSA-mPEG was dried overnight in vacuum at room temperature (81.4% yield)[48].

2.3. Characterization of the pre-polymer and copolymer

The chemical structure of pre-polymer and block copolymer was confirmed by ^1H NMR and the spectrum was recorded with a Bruker DRX 500 MHz spectrometer. A 1 wt % polymer solution in $CDCl_3$ was used for the measurement.

FTIR spectroscopy was done by a Perkin Elmer spectrum one spectrometer to confirm the chemical structure of PSA, PSA-mPEG and its degradation products. The polymer samples pellets were prepared using KBr.

Number average molecular weight (M_n), weight average molecular weight, and polydispersity index (PDI) of the synthesized block copolymer were measured by gel permeation chromatography (GPC) (Measurements were done at KTH) using

polymethylmethacrylate (PMMA) as standard for calibration. Measurements were done in triplicate and the results are reported in average.

2.4.*In vitro* hydrolytic degradation

The degradation study of PSA-mPEG was performed in 10 ml phosphate saline buffer (PBS) of pH 7.4. Three samples containing 200 mg polymer were prepared for three time intervals. The samples were placed in an incubator shaker (Edmund Bühler GmbH model TH30) at 75 rpm and 37°C. A 1-ml aliquot of PBS was replaced by fresh PBS every 24 hours. After 3 days the PBS in the first sample was removed and then lyophilized and kept at -80°C . The second sample was treated with the same procedure after 6 days and the third one after 10 days. The degradation products were further characterized by FTIR spectroscopy. The first and third samples were chosen to investigate the change in molecular weight by GPC. Measurements were done in triplicate and the average molecular weight was reported.

2.4.1. Phosphate buffer saline (PBS) preparation

PBS was prepared by dissolving 2.175 g $NaCl$, 0.068 g KH_2PO_4, and 0.284 g Na_2HPO_4 in 200 ml deionized water. The pH was adjusted to 7.4 either by adding 1N HCl or 1N$NaOH$. The final volume was then brought to 250 ml by adding deionized water[49].

2.5.Nile red loaded nanoparticles

To evaluate the drug loading properties of PSA-mPEG nanoparticles, nile red was used as a hydrophobic drug model. This drug model was encapsulated within PSA-mPEG nanoparticles by nanoprecipitation method. Nile red stock solutions of 0.005 (w/v) % and 0.01 (w/v) % in tetrahydrofuran (THF) were prepared. PSA-mPEG (20mg) was dissolved in 4600 μl THF and 400 μl nile red (0.01 (w/v) %) was added to the polymer solution. From 0.005 (w/v) % nile red stock solution, 300 μl was added the same way to 4700 μl of polymer solution in THF containing 20 mg PSA-mPEG.

The organic solution containing dye and polymer was added drop-wise by needle and syringe to 15 ml filtered (0.1 μm MILLEX® VV) deionized-water (non-solvent) under magnetic

stirring at room temperature. THF was removed afterwards by a rotary evaporator. Resulting nile red-loaded nanoparticles were recovered by ultra-centrifugation (Beckman L-80 XP ultracentrifuge) for 1 hour with 25000 r.p.m at 4°C . The supernatant which contained non-encapsulated nile red was discarded and nanoparticles were then lyophilized and stored at 4°C.

2.6. Nile red encapsulation efficiency and content

The amount of nile red entrapped in PSA-mPEG nanoparticles was measured by HPLC (Perkin Elmer Series 200). 1 mg of accurately weighted nanoparticles was suspended in 1 ml of ethanol to extract the encapsulated nile red. For complete extraction, the suspension was sonicated for 10 minutes and the nanoparticles were separated by a spin down centrifuge. The amount of encapsulated nile red was measured by injecting 10 μl of supernatant and detection at 550 nm using a calibration curve made based on peak area and absolute amount of nile red. HPLC measurements were done at analytical chemistry group at UIO.

$$encapsulation\ efficiency(\%) = \frac{amount\ of\ nile\ red\ in\ naoparticles}{initial\ amount\ of\ nile\ red} \times 100$$

$$Dye\ Content\left(\%\frac{w}{w}\right) = \frac{amount\ of\ nile\ red\ in\ nanoparticles}{amount\ of\ nanoparticles} \times 100$$

2.7. SPIO loaded polymeric nanoparticle preparation

SPIO loaded polymeric nanoparticles (SPIO-PNPs) were prepared by the nanoprecipitation method using PSA-mPEG as the polymeric vehicle. SPIO-NPs had an average diameter of 10 nm and the surface of the particles was hydrophobically modified with oleic acid. SPIO-NPs (5 mg/ml) in THF (sample 1=40 μl, sample 2=80 μl, sample 3=120 μl, sample 4= 160 μl) were added to the solution of 20 mg PSA-mPEG in THF (sample 1=4.960 ml, sample 2=4.920 ml, sample 3=4.880 ml, sample 4= 4.840 ml). Later, the suspensions were added drop-wise to 15 ml of filtered deionized water (0.1 μm MILLEX® VV) by needle and syringe under constant stirring of an overhead stirrer at 900 r.m.p (Ruhrwerk EUROSTAR power control-visc P7). THF was further removed by a rotary evaporator (Figure 2-1).

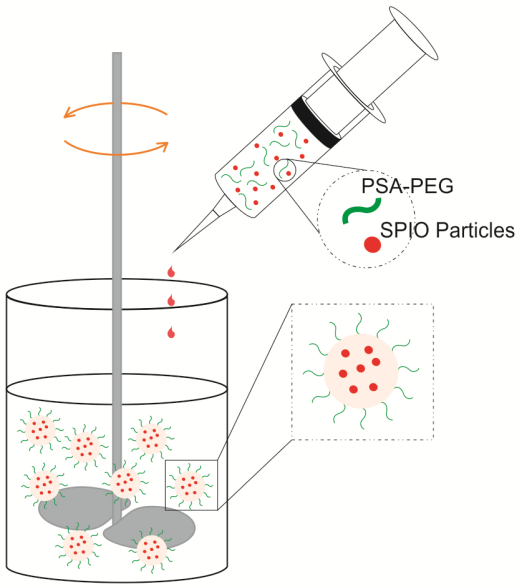

Figure 2-1: Schematic of SPIO-NPs loaded in PSA-mPEG by nanoprecipitation method

2.8. Purification of SPIO loaded nanoparticles

After solvent removal, nanoparticles were collected by ultracentrifugation (Beckman L-80 XP ultracentrifuge) at 25000 r.p.m for 60 minutes at 4°C. The supernatant was discarded and the nanoparticles were suspended in 4 ml solution of 0.05 MHNO_3. In order to remove unloaded SPIO-NP, the suspension was neutralized with PBS pH 7.4. The resulting iron hydroxide aggregates were eliminated by mild centrifugation (2000 r.p.m for 15 minutes). The loaded SPIO-PNPs in the supernatant were collected by ultracentrifugation (27000 r.p.m for 90 minutes at 4°C and re-suspended in 5 ml of deionized water [50].

The resulting suspension was stored for studying its size, morphology and zeta potential while for studying iron oxide content of SPIO-PNPs the suspension was lyophilized and stored at 4°C for further measurement.

2.9. Inductively coupled plasma spectroscopy (ICP-MS) analysis

Iron content of SPIO-PNPs was measured using ICP-MS. Analysis was performed using a

Thermo Finnigan Element 2 instrument (Bremen, Germany). The measurements were done at chemistry department of NTNU.

To correlate the iron concentration obtained from ICP-Ms analysis to the amount of iron oxide particles, the following relation was used[29] :

1 particle of SPIO = 62896 iron atoms

1 g of SPIO-NPs = 1.71×10^{17} particles

The iron oxide content in SPIO loaded polymeric nanoparticles is calculated by the below relation [50] :

$$Iron\ oxide\ conten(\%) = \frac{mass\ of\ iron\ oxide\ in\ SPIO - PNP}{mass\ of\ SPIO - PNP} \times 100$$

2.10. Dynamic light scattering (DLS)

DLS measurements were carried out to determine the size of SPIO-PNPs. The experiments were conducted using an ALV/CGS-8F multi-detector compact goniometer system with eight off fiber-optical detection units made by ALV-GmbH, Langen, Germany. The laser light (He-Ne,λ = 632.5 nm) was focused on the sample cell (10 mm NMR tube). The temperature control of the cell was provided by a thermostat, circulating water around a cylindrical quartz container filled by a refractive index-matching liquid (*cis*-decalin). The intensity of scattered light from the sample measured simultaneously at eight scattering angles in a range of 22-141°. All the sample solutions were filtered in the atmosphere of filter air through a 5 μm filter (Millipore) into the pre-cleaned NMR tubes to avoid entering dust to the solutions.

2.11. Transmission electron microscopy (TEM)

The morphology of nanoparticles was investigated by TEM. For this, the suspension of particles was absorbed on hexagonal copper grids for 2 minutes followed by washing three times with MQ-water and further staining with 3% uranyl acetate. The imaging was

performed with a Philips transmission electron microscope CM100 (Philips, Eindhoven, The Netherlands). The images were recorded digitally with a Quesma TEM CCD camera (Olympus Soft Imaging Solution, Germany) and iTEM software (Olympus Soft Imaging Solution, Germany).

2.12. Zeta potential

The zeta potential measurements were conducted on a Malvern Zetasizer Nano ZS (Malvern Instrument Ltd. Worcestershire, UK). The sample cell used was a dip-cell, including palladium electrodes with 2mm spacing, one PCS115 cuvette, and a cap. First standard solution of -68 mV was measured three times after that measurements continued on 600μl of sample solutions in triplicate.

2.13. *In vitro* cytotoxicity

MDA-MB-231 breast cancer cells were used to determine the cell cytotoxicity. The cells were cultured in RPMI 1640 cell culture medium (Lonza, Verviers, Belgium) containing 10% fetal bovine serum and 1% penicillin-streptomycin. Cells were grown by incubation in T75 flask at 37°C in humidified atmosphere with 5% CO_2. After getting enough confluence, 1ml trypsin with a concentration of 200 mg/l was added to dissociate the cells. Trypsin was further neutralized by 5 ml of cell culture medium.

To obtain the number of viable cells per milliliter, 100 μl of cell suspension was mixed with 100 μl of trypan blue solution, subsequently 10 μl of this solution was added to a cell counting chamber and viable cells were counted three times under the microscope at 1000 magnification. Under the microscope a grid of 9 squares is visible. The microscope then should be focused on one of the 4 outer squares in the grid (Figure 2-2) which contains 16 smaller squares. The unstained cells are counted in this square. Nonviable cells are stained by trypan blue while viable cells remained unstained. The average of these three time readings was multiplied by 10^4 to obtain the number of viable cells per milliliter[51]. The three readings for trypan blue assay were 61, 62 and 67 therefore the average concentration of viable cell was 63× 10^4 $cell/ml$.

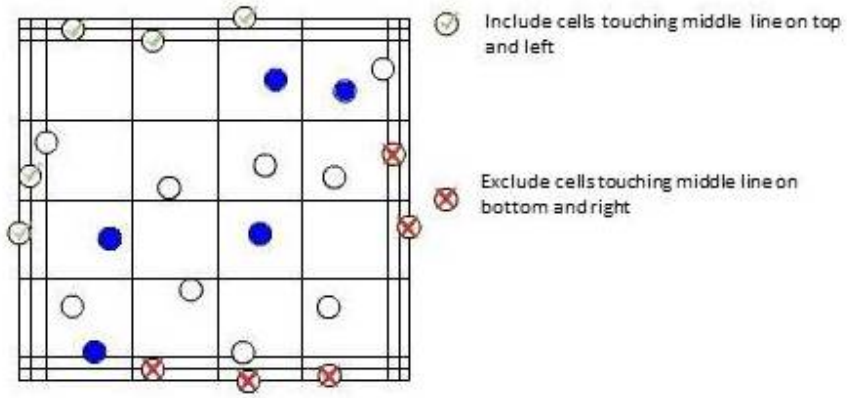

Figure 2-2 : Cell counting by trypan blue assay using a cell counting chamber

Harvested cells were seeded in a 96-well plate at the density of 5×10^3 viable cells /well. According to trypan blue assay results, the required density of viable cells corresponds to 175 μl cells for 20 wells. This amount was added to 1825 μl cell culture medium and 100 μl of this mixture was seeded in each 20 plates followed by 24 hours incubation at 37°C in humidified atmosphere with 5%CO_2. To reduce evaporation during incubation, cell-seeded wells were surrounded by wells contacting 200 μl of culture medium. Blank PSA-mPEG NP (PNP), SPIO-NP and SPIO-PNP suspensions were made by adding lyophilized nanoparticles to cell culture medium with concentration ranging from 1 to 2 μg/ml. 24 hours post incubation, 100μl of nanoparticle solutions were added to the wells with seeded cells according to the Figure 2-3.

Cell viability of nanoparticle treated cell was assessed by MTS [3-(4, 5-dimethylthiazol-2-yl)-5-(3-carboxymethoxyphenyl)-2-(4-sulfophenyl)-2H-tetrazolium] assay. 20 µl MTS (CellTiter 96® Promega, Madison-USA) was added to each cell and incubated for 3 hours. The cell viability was further determined at three time intervals (24 hours, 48 hours and 72 hours). This method is based on bio-reduction of tetrazolium salt to an intensely colored formazan with UV absorbance at 490 nm. The quantity of formazan product measured by UV spectroscopy is directly proportional to the number of living cells. The absorbance of the

produced formazan was measured by plate reader at 490 nm (Wallac Victor, Turku-Finland). The cell viability was calculated using following formula:

$$cell\ viability(\%) = \frac{absorbance\ of\ treated\ cells}{absorbance\ of\ untreated\ cells} \times 100$$

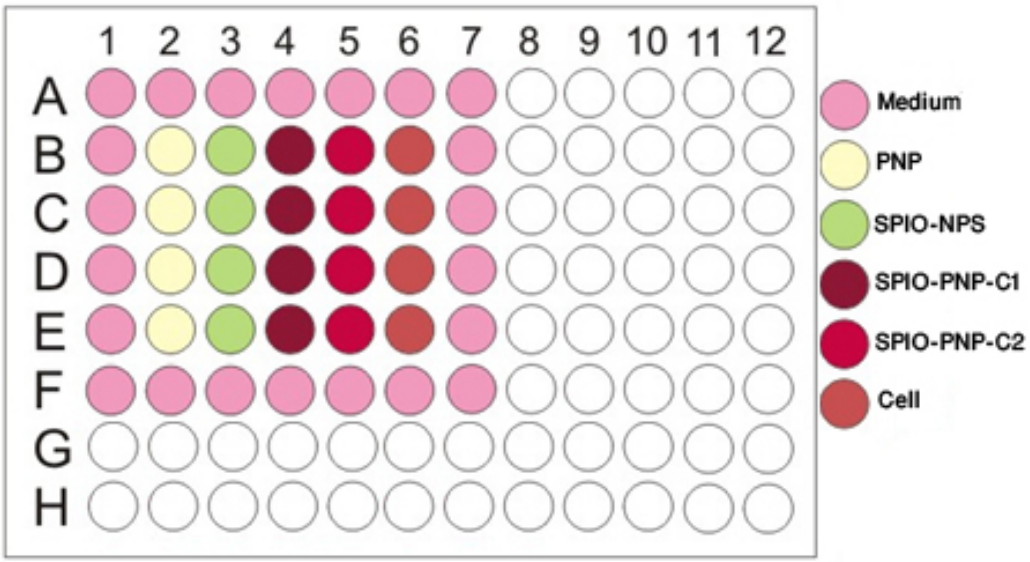

Figure 2-3 : Cell seeding pattern in 96-well plate

2.14. *In vitro* Cellular uptake of SPIO loaded nanoparticle

To assess cellular uptake of SPIO loaded PSA-mPEG (SPION-PNPs) nanoparticles, the MDA-MB-231 cancer cells were seeded in 6-well plate at a density of 6×10^6. The cells were allowed to grow for 24 hours; subsequently, the medium was replaced by fresh medium containing SPION-PNPs nanoparticles. 24 hours post addition of nanoparticles the medium was removed and the cells were washed with 1 ml PBS. The cells were fixed by 2% glutaraldehyde in cacodylate buffer pH 7.0 and left overnight at 37°C and then cross-sectioned in department of biology at UIO. The cross-sectioned cells were imaged by TEM afterwards.

3. Results and discussion

3.1. Characterization of pre-polymer and block copolymer

The chemical structure of PSA-mPEG block-copolymer and PSA pre-polymer is confirmed by ^1HNMR and FTIR spectra (Figure 3-1) and (Figure 3-2). The chemical shifts at δ=1.3, 1.6, 2.2, and 2.4 ppm are well resolved and correspond to hydrogen atoms of PSA functional groups. The peak at δ=3.6 ppm is assigned to the methylene protons on the PEG block which was introduced by block-copolymerization. Another chemical shift observed at δ=4.2 ppm belongs to the methylene protons of glycol next to the ester bond of sebacic anhydride and ethylene oxide. This can confirm the successful polymerization of PSA and PEG. [42].

The FTIR spectra of sebacic acid (SA), poly (sebacic anhydride) (PSA), and poly (sebacic anhydride)-*block*-methyl ether poly (ethylene glycol) (PSA-mPEG) are illustrated (Figure 3-2). It reveals that absorption peaks related to asymmetric and symmetric stretching modes of carbonyl groups in anhydride segment developed at 1740 and 1813 cm^{-1} while corresponding peaks of asymmetric and symmetric stretching modes of C-O for anhydride segments appear at 1074 and 1041 cm^{-1} respectively. The peaks at 2935-2915 cm^{-1} and 2854-2840 cm^{-1} are assigned to the methyl and methylene vibrations. Absorption peaks at 960 $cm^{-1}$and 1100 corresponds to symmetric and asymmetric stretching modes of C-O-C of ethylene glycol [42, 47].

The average M_n and M_w obtained from GPC were 2497 and 2929 g/mol respectively and the PDI was 1.17.

3.2. *In vitro* hydrolytic degradation of PSA-mPEG

PSA-mPEG undergoes hydrolytic degradation via surface erosion of PSA block in PBS buffer at 37°C. The conversion of anhydride bonds to acid groups is depicted in FTRI spectra of degraded polymers (Figure 3-2). During the degradation a strong carboxylic hydroxyl band appears between 2500 and 3300 cm^{-1}. This is followed by appearance of a carboxylic

carbonyl band at 1704 cm^{-1}which its intensity becomes stronger with degradation time. Meanwhile the characteristic peaks for anhydride segment at 1813 and 1740 $cm^{-1}$and C-O-C stretching band at 1100 cm^{-1}become weaker (Figure 3-3) [47, 52].

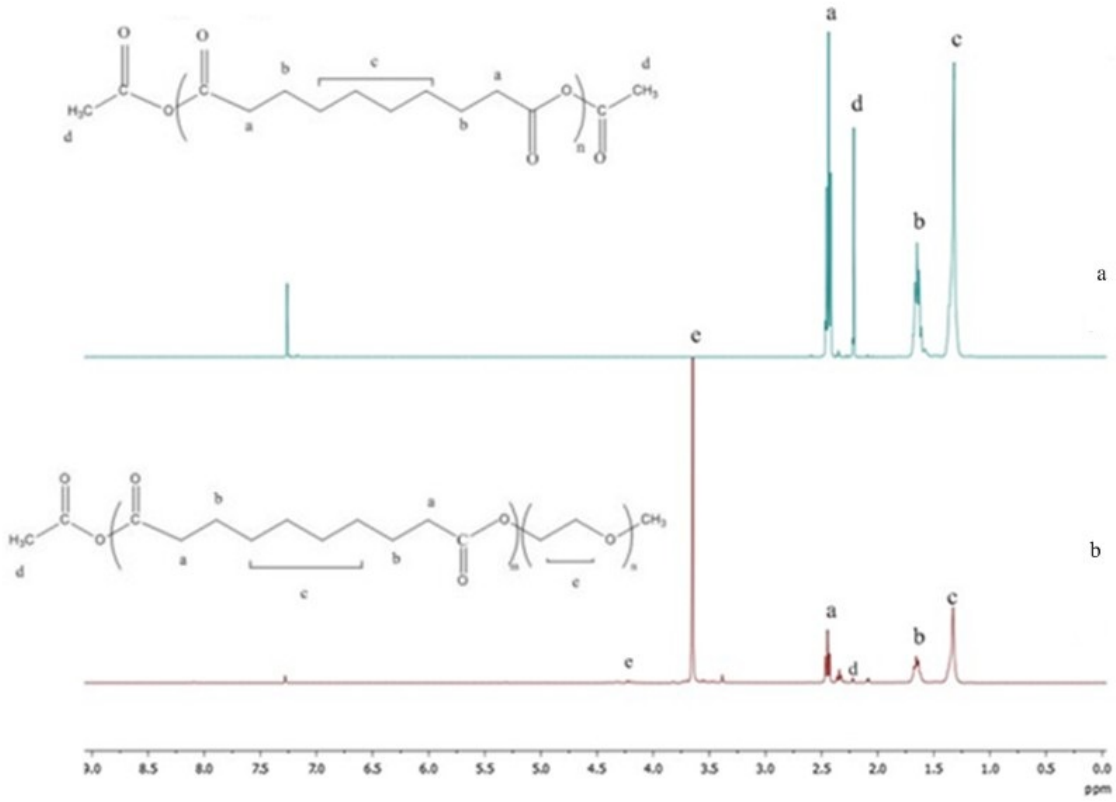

Figure 3-1 $^{1}HNMR$ **spectra of (a) PSA and (b) PSA-mPEG**

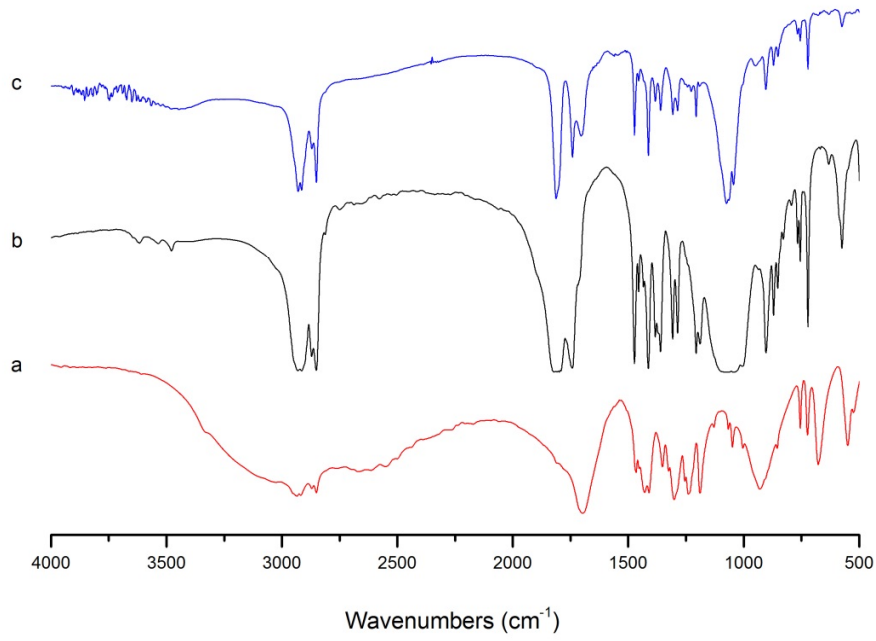

Figure 3-2 FTIR spectra of (a) sebacic acid (SA), (b) poly (sebacic anhydride) (PSA), (c) Poly (Sebacic anhydride)-*block*-methyl ether poly (ethylene glycol) (PSA-mPEG)

To monitor the degradation rate, the change in molecular weight was studied by GPC. Molecular weight (M_w) of three time intervals is shown in Figure 3-4. After 3 days there was a 14% loss in molecular weight, this amount reached 23% after 10 days. Due to the surface erosion mechanism of poly (sebacic anhydride) block, the polymer was able to maintain 77% of its initial molecular weight after 10 days. This makes the this block copolymer applicable for controlled drug delivery and can provide a sustained release over long period of time[53].

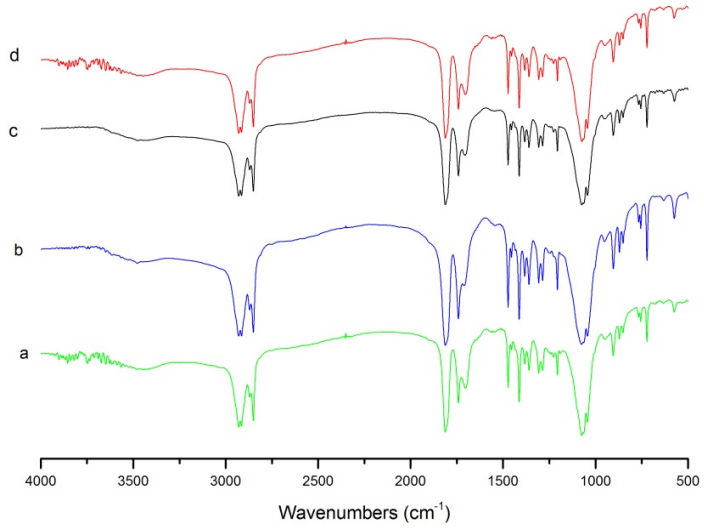

Figure 3-3 FTIR spectra of degradation of PSA-mPEG at (a) 0 day (b) 3rd day, (c) 6th day, and (d) 10th day

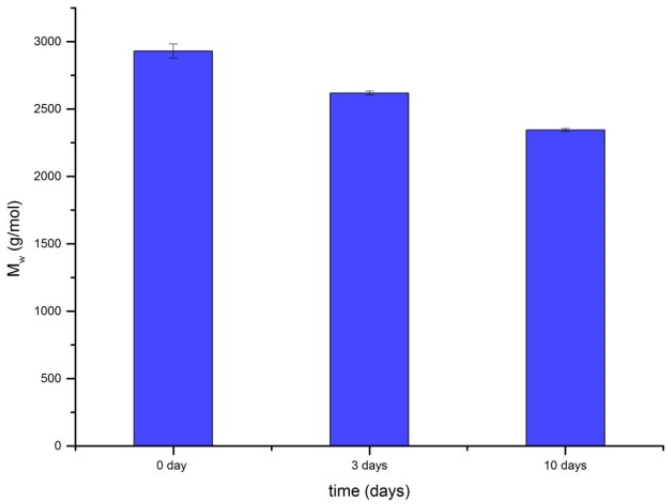

Figure 3-4 : Change in molecular weight (M_w) by hydrolytic degradation

3.3. Encapsulation efficiency

The resulting encapsulation efficiency and dye content of nile red is summarized in Table 1.

Table 1 : Characters of nile red loaded in PSA-mPEG nanoparticles by nanoprecipitation method

Initial amount of dye (μg)	Dye-polymer ratio (%)	Encapsulation efficiency (%)	Dye content (%)
15	0.075	59.1	0.15
40	0.2	55.7	0.3

As it is shown in the table above the drug content was predictably higher for larger initial dye usage but despite the big difference in initial dye amount of the two dye-polymer ratios there was not a big difference in encapsulation efficiencies. One should note that inevitably small amount of nanoparticles may be lost during the washing process which may have a slight impact in the resulting encapsulation efficiency and dye content.

3.4. Synthesis of SPIO-loaded polymeric nanoparticle (SPIO-PNP)

Purified SPIO-PNPs were prepared with four different loading levels of SPIO (w/w based on polymer): 1%, 2%, 3% and 4% by nanoprecipitation method. Table 2 summarizes size, and SPIO content of the prepared SPIO-PNPs.

The average diameter of SPIO-PNPs seems to be affected by amount of SPIO encapsulated in these particles. SPIO content of nanoparticles and their average diameter was at its maximum for 2% SPIO loading whereas 4% SPIO loading which had the minimum SPIO content corresponds to the smallest diameter. 1% and 3% SPIO loading with close amount of SPIO content had approximately the same size. The same relation between therapeutic agent content and size of a nanoparticle was observed in a previous study[54].

Table 2 : Characters of SPIO-NPs loaded in PSA-mPEG by nanoprecipitation method

SPIO loading (%)	Diameter size(nm)	SPIO content (%)
1	188	0.05
2	266	0.08
3	216	0.03
4	154	0.01

The size of tumor vascular pores may vary from 100 to 600 nm[55] and carrier systems with diameter larger than 200 nm may induce nonspecific scavenging by reticuloendothelial system (RES)[56], consequently particles with diameters less than 200 nm exhibit improved EPR effect[57]. Considering this fact and the SPIO content of the synthesized nanocarriers in Table 2, 1% SPIO loading seems to be an optimal platform for cancer therapy applications.

In Figure 3-5, normalized time correlation function data at 5 scattering angles for the samples in Table 2 together with the corresponding curves fitted by equation 4 are illustrated. For all four samples the relaxation process is unimodal and the correlation function was fitted successfully by the first stretched exponential function in equation 4. The average β value was 1 for all samples except for 3% SPIO loading, where the value was 0.9.

In Figure 3-5 the decay rate (τ^{-1}) as a function of q^2 is also depicted, which discloses the diffusivity of the system; the slope of this plot represents the apparent diffusion coefficient D, which in diffusive systems is not dependent on scattering angle. By putting D in equation 8 the hydrodynamic radius (R_h) is determined.

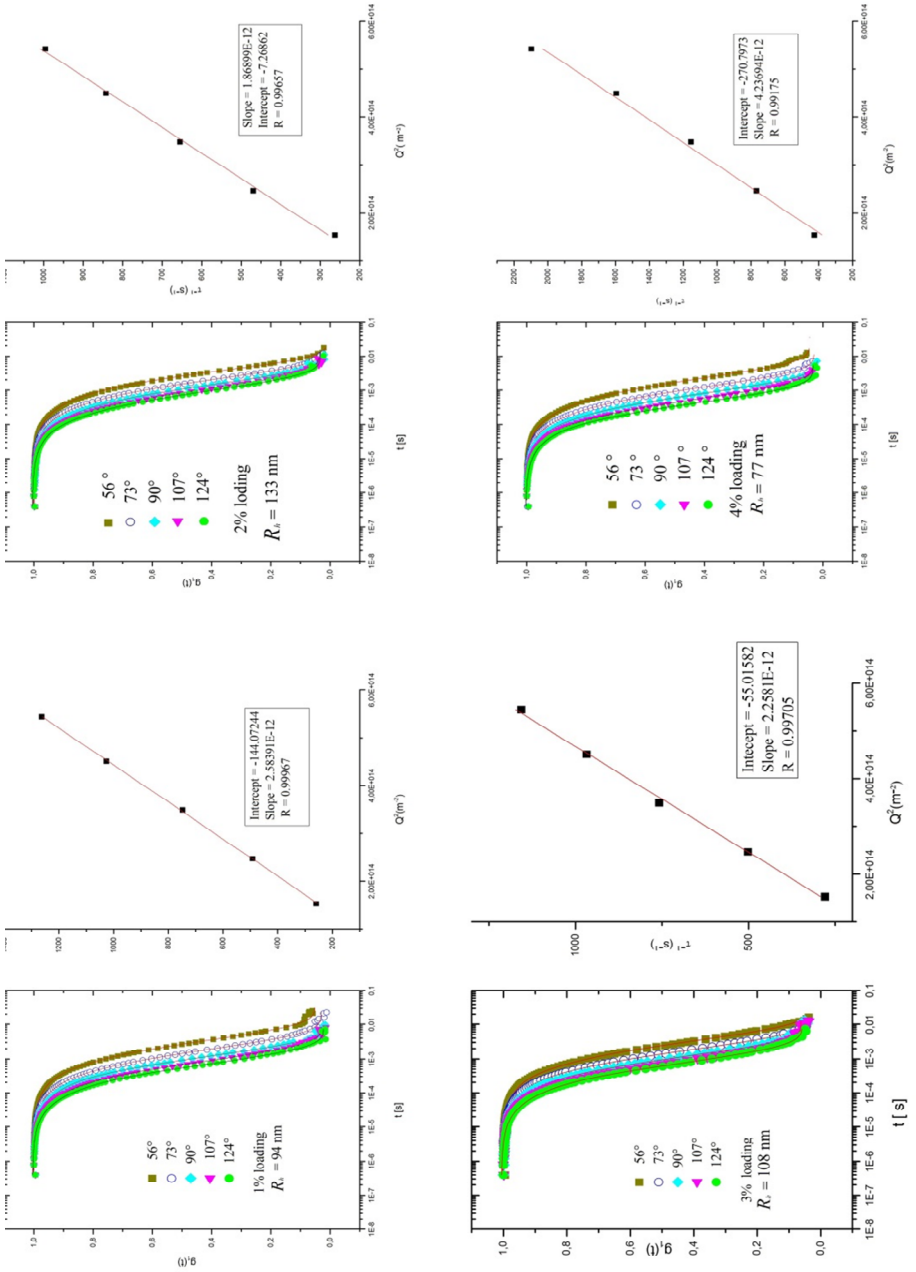

Figure 3-5 : First-order electric field correlation function vs. time and the decay rate (τ^{-1}) as a function of q^2 for 1%, 2%, 3% and 4%SPIO loading of SPIO-PNP solutions.

3.5. Zeta potential

To explore the stability of SPIO-NPs after encapsulation with PSA-mPEG zeta potential measurement was conducted on SPIO-PNPs with four concentration of SPIO (1%, 2%, 3% and 4%), blank PSA-mPEG nanoparticle (PNP) and SPIO nanoparticle without encapsulation (SPIO-NP) (Figure 3-6) in deionized water and PBS.

Figure 3-6 shows no sign of significant decrease in zeta potential after encapsulation with polymer and it seems that the nanoparticles are stable before and after encapsulation with polymer due to the fact that the absolute value of zeta potential is high (larger than 30 mV) and the particles can be assumed to be electrostatically stabilized. Blank PSA-mPEG nanoparticles with zeta potential value about -15 mV on the other hand seems to be considerably less stable than SPIO loaded PSA-mPEG nanoparticles [44].

The absolute value of zeta potential decreased considerably after re-suspending SPIO-PNPs in PBS. This might be due to the increase in ionic strength of the system which leads to gradual screening of electrostatic repulsive forces [58].

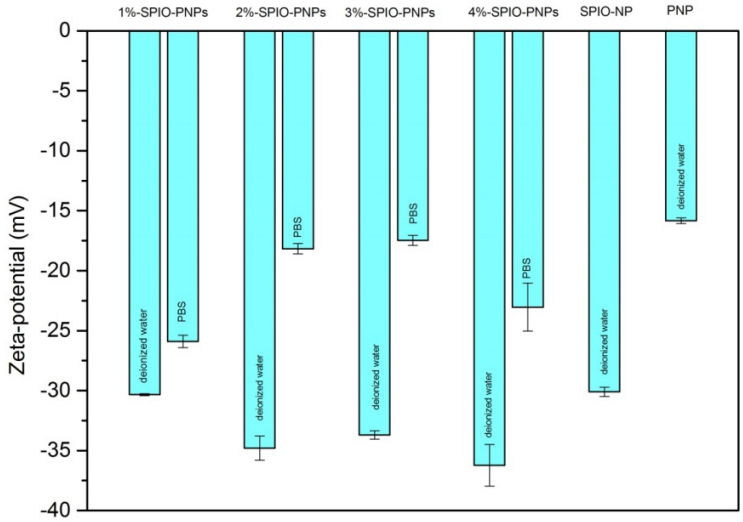

Figure 3-6: Zeta potential measurement of SPIO-PNP, SPIO-NP and PNP

3.6. Long term stability of SPIO-loaded polymeric nanoparticles (SPIO-PNP)

DLS was employed to measure the size of (SPIO-PNP) over course of 30 days at room and body temperature. The hydrodynamic radius derived from the fast relaxation time during the period of one month is depicted for 1% SPION-PNPs in Figure 3-7.

The hydrodynamic radius of nanoparticles did not change considerably over time so it can be concluded that particles were stable during the time period [59]. Steric repulsion between highly negatively charged particles along with the amphiphilic structure of the di-block copolymer can probably be named as the main reason for the stability of nanoparticles. Due to the surfactant-like behavior of amphiphilic di-block copolymers nanoparticles can be prepared by nanoprecipitation method without using stabilizers such as poly (vinyl alcohol) (PVA). Stabilizers are usually hard to remove and may cause toxicity [60].

In Figure 3-8, normalized time correlation function data at scattering angle of 107° together with corresponding fitted curves by equation 4 are illustrated in the form of semilogarithmic plots for aqueous suspension of 1% SPIO-PNPs. The measurements were done at 6 time intervals at temperature 25 and 37 °C . The decay curves fitted by aid of equation 4 can be described by a stretched exponential with($\beta>0.95$) (Table 3) indicating almost a single exponential decay and a narrow size distribution [61].

In the normalized correlation functions for the 15th day with corresponding unimodal fitted curves at 5 scattering angles are depicted for both temperatures (Figure 3-9). The slope of decay rate (τ^{-1}) as a function q^2 probes diffusion coefficient which was used to calculate the hydrodynamic radius of the particles. The linear correlation coefficient, R close to 1 is also a rather clear indication of the dominance of diffusion as a main relaxation mechanism of the system.

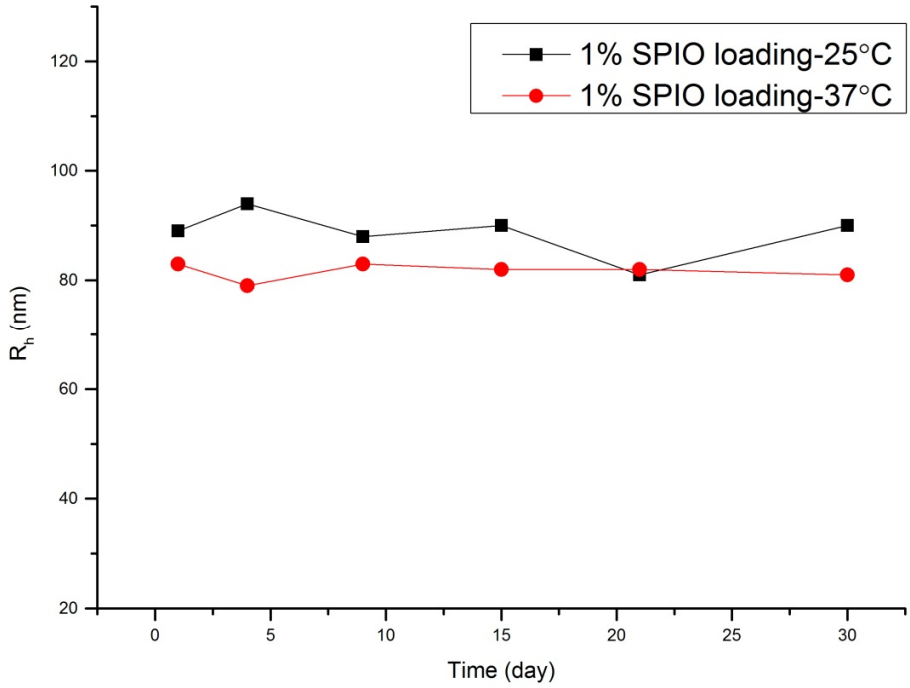

Figure 3-7 : Hydrodynamic radius of 1%loading SPIO-PNPs at 25 and 37℃ over one month

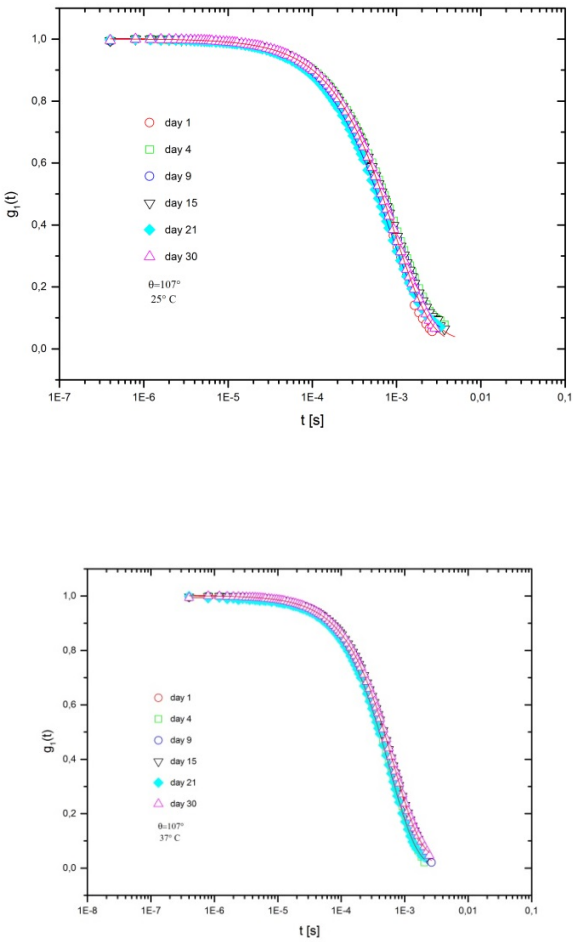

Figure 3-8 : normalized time correlation function data at scattering angle of 107°for solution of 1%loading SPIO-PNPs at 25 and 37℃ .The curves are fitted with the aid of equation 4

Table 3 : β value obtained from fitting curve of correlation function at angle of 107° at 25 and 37℃.

	Day1	Day4	Day9	Day15	Day21	Day30
25℃	1	0.97	0.96	0.95	0.97	1
37℃	0.97	1	0.98	0.98	1	0.98

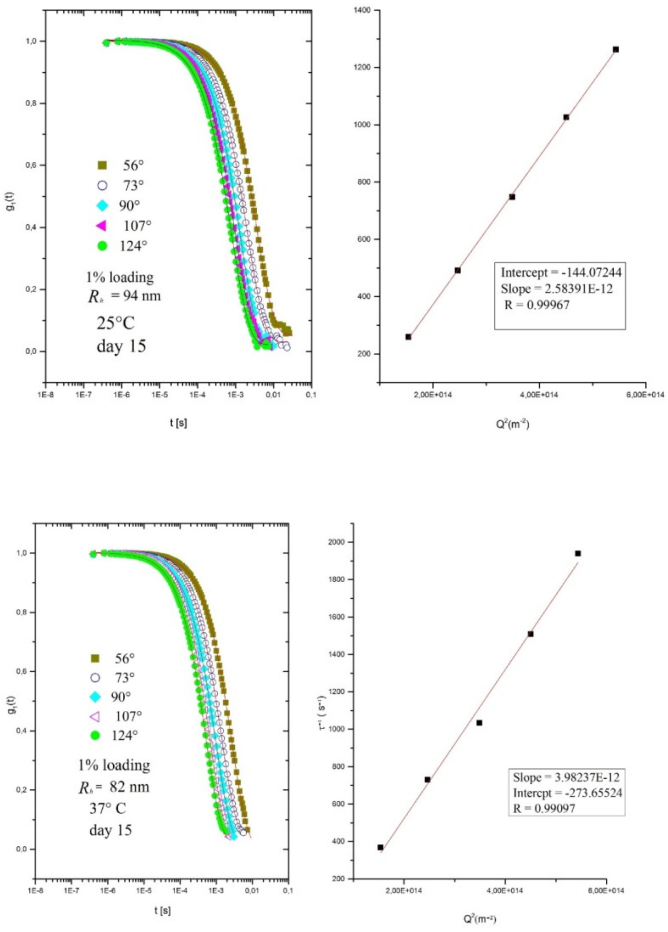

Figure 3-9: First-order electric field correlation function vs. time and the decay rate (τ^{-1}) as a function of q^2 for 1% loading SPIO-PNP solution at 15th day

3.7. Transmission electron microscopy (TEM)

The successful encapsulation of SPIO nanoparticles in polymer shell was visualized by Figure 3-10(a-c) shows iron oxide nanoparticle encapsulated in polymer shell. The electron dense iron oxide nanoparticles are clearly seen as dark regions in the micrograph which are surrounded by a gray-shaded polymeric shell [62]. The morphological observation of SPIO loaded polymeric nanoparticles by TEM shows roughly round-shaped nanoparticles. It should be mentioned that in morphological studies by TEM one should consider that TEM micrograph is not representative of the real state of nanoparticles in suspension since the dispersion medium is removed during sample preparation and the ''grape-like'' organization of the particles in micrographs could be a consequence of that [63].

3.8. Cytotoxicity

Apart from their supermagnetic properties, SPIO-NPs have attracted considerable attention due to their low toxicity in human body. A study conducted on breast cancer cells revealed that iron oxide nanoparticles coated with a surfactant are non-toxic in concentration range of 0.1-10 μg/ml while the particles show toxicity at 100 μg/ml[64].

One of the mechanisms by which iron overload can induce toxicity is via producing highly reactive hydroxyl radicals. SPIO-NPs are presumably degraded into iron ions by hydrolyzing enzymes. These iron ions can potentially pass the mitochondrial membrane and react with hydrogen peroxide and oxygen produced by mitochondria. This leads to formation of highly reactive hydroxyl radicals that could damage DNA, proteins, polysaccharides and lipids *in vivo* [65].

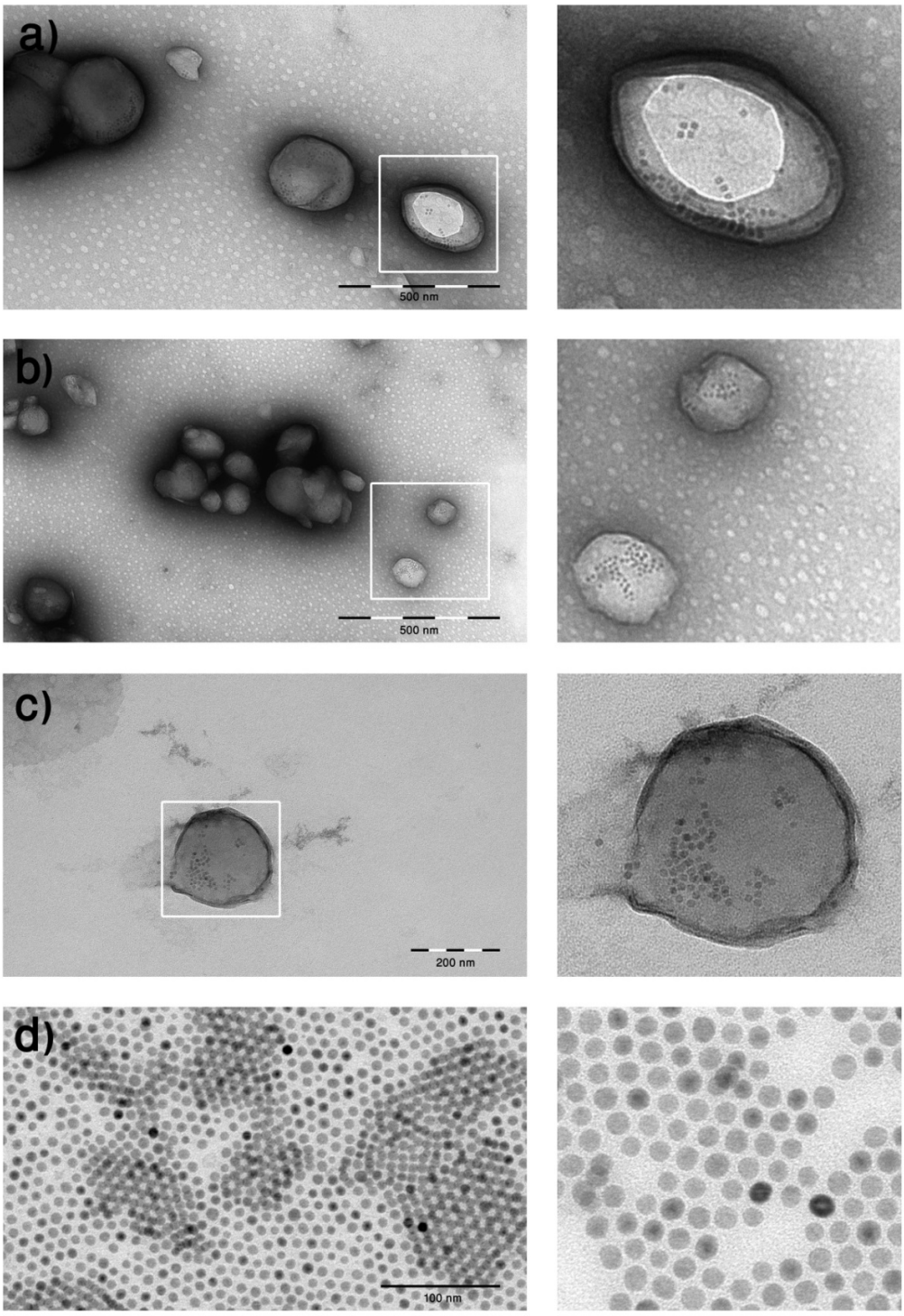

Figure 3-10 : TEM image of (a-c) iron oxide nanoparticles encapsulated in polymer matrix (SPIO-PNP) (d)super-paramagnetic iron oxide nanoparticles(SPIO-NPs)

Both SPIO and SPIO loaded polymeric nanoparticles showed negligible cytotoxic effect in the concentration range of 1-2 μg/ml up to 72 hours (Figure 3-11). The results within this concentration range are consistent with the previous work done on breast cancer cell lines [64]. The results also indicate that the oleic acid used as stabilizer on surface of SPIO-NP did not trigger toxicity.

Cell viability of blank PSA-mPEG nanoparticles was also high (>85%) which is in agreement with the previous studies on sebacic anhydride copolymers [66] and makes this polymer a safe carrier for SPIO-NPs. Another interesting feature demonstrated by blank PSA-mPEG nanoparticles is their high cell viability after 72 hours which could be an indication of low toxicity of degradation products of PSA-mPEG copolymer since it has been shown in this study that *in vitro* hydrolytic degradation of the copolymer has been started after 3 days.

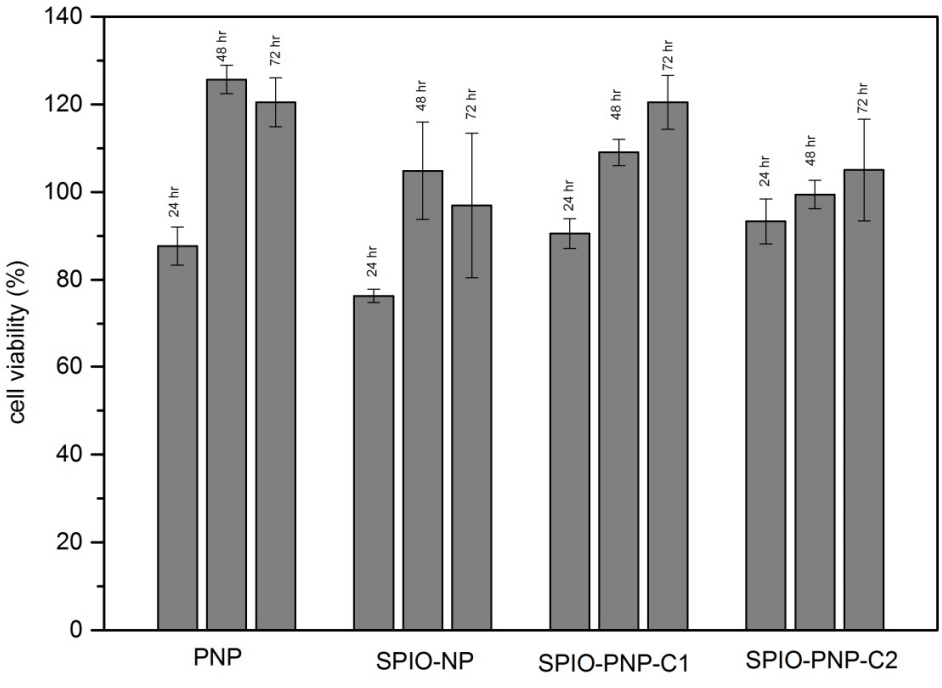

Figure 3-11 : Cell viability of blank PSA-mPEG nanoparticles (NP), SPIO-NP and SPIO-PNP with two concentrations (c1 and c2)

3.9. Cell uptake

Since accumulation of nanoparticles in cancer cells is of great importance for cancer detection and treatment, TEM study on MDA-MB-231 human breast cancer cells was performed to visualize the presence and confinement of SPIO-PNPs within the cancer cells. To confirm that the nanoparticles were indeed internalized by target cells rather than simply binding to the surface of the cells, the nanoparticle treated cells were embedded then cross sectioned and studied by TEM.

TEM images confirmed that SPIO-PNPs with average diameter between 150-200 nm crossed the cell membrane via endocytic pathway and internalized inside vesicles. Endocytosis is a mechanism by which mammalian cells internalize small molecules, macromolecules, and particles and target them to sealed organelles within the cytoplasm[67]. Observing this internalization via endocytosis is compatible with the previous research done to investigate SPIO-PNPs uptake by breast cancer cells [27]. Furthermore as predicted from cytotoxicity experiments cancer TEM observations showed that cellular structures were well preserved and no visible abnormalities were observed in cells treated with SPIO-PNPs.

Cell uptake is described as a two-step process: the first step is binding to the cell membrane, via cell surface receptors and the second is the actual internalization event [68]. The first step is demonstrated in Figure 3-12-b which shows a particle binding to the cell membrane before crossing it. In Figure 3-12-c and d one can clearly recognize the second step of the cell uptake process which is the successful internalization of particles within vesicles of diameter between 1.5-2 μm. Figure 3-12-a is the image of control cell.

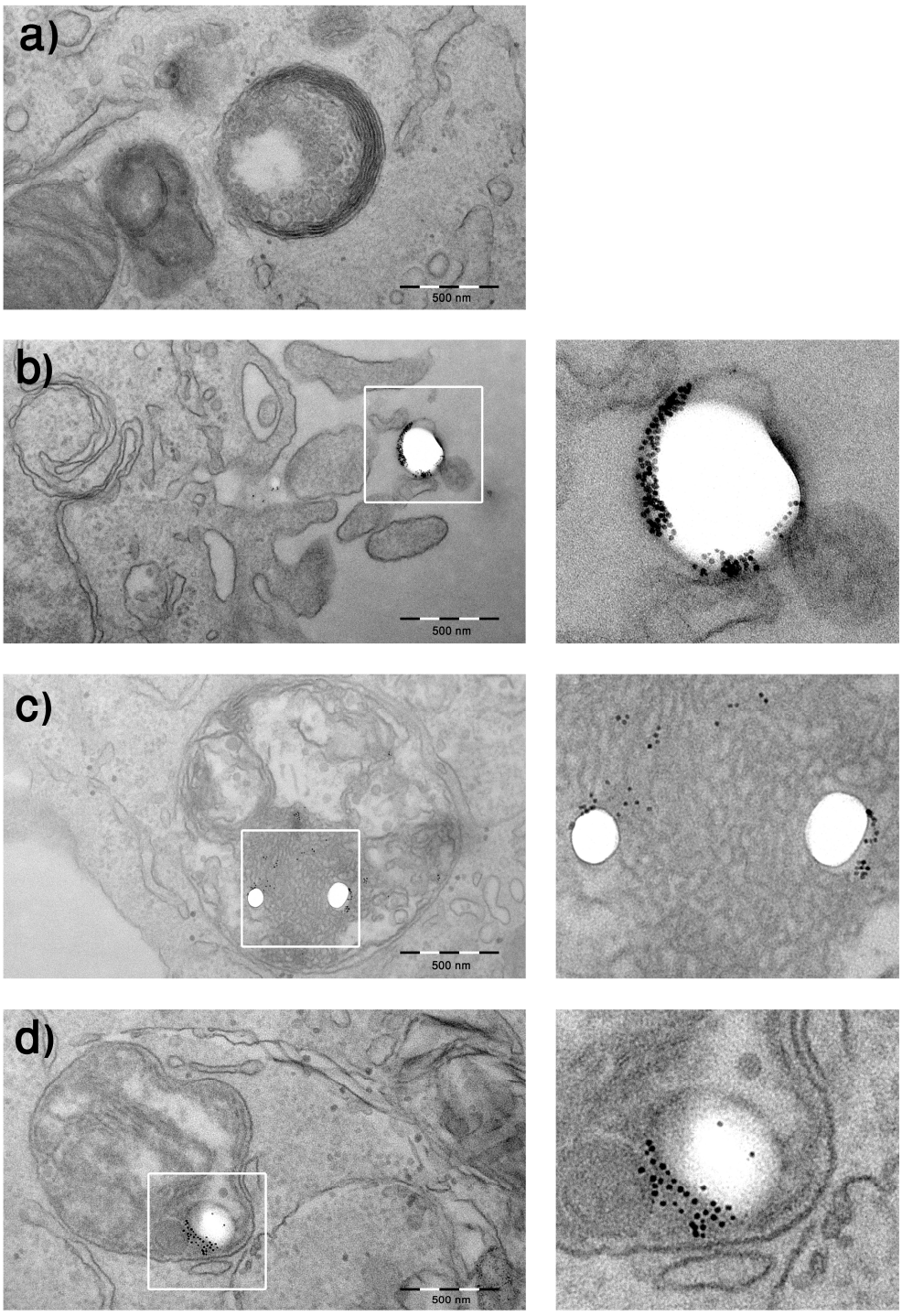

Figure 3-12 : TEM image of (a) control cell (b) particles before crossing the cell membrane (c-d)after confinement within the cell.

4. Conclusion

Block copolymer of poly (sebacic anhydride)-*block*-methylether-poly (ethylene glycol) (PSA-mPEG) was synthesized via melt-condensation. The polymer was characterized using ^1H NMR and FTIR which verified the success of copolymerization. The molecular weight ($M_w and\ M_n$) and poly dispersity index (PDI) were obtained by GPC.

The degradation behavior of (PSA-mPEG) was studied in PBS at pH 7.4 at 37°C. As the degradation preceded conversion of anhydride bonds to acid and weakening of anhydride linkage was observed in FTIR spectra. The change in molecular weight was also investigated during the degradation. After 3days the polymer maintained 86% of its initial molecular weight this reached to 77% after 10 days.

Nile red was encapsulated as a hydrophobic drug model. The encapsulation efficiency and dye content was measured by HPLC. The main focus of this study was encapsulation of SPIO-NP within a biodegradable and biocompatible polymer synthesized in this research. The successful loading of SPIO-NPs in the polymer shell was confirmed by TEM. The size and SPIO-NPs content for four polymer-SPIO ratios were studied to find an optimal carrier system for cancer therapy applications. Considering the required size for reaching the tumor site, 1% SPIO loading was recognized to be a good carrier of choice.

Zeta potential of SPIO-PNPs, SPIO-NPs and blank PNPs were investigated in deionized water and PBS. No considerable change of zeta potential for SPIO-NPs was observed after encapsulation with polymer shell and all the carriers except PNPs had enough surface charge to be stable in deionized water. The value of zeta potential of SPIO-PNPs decreased after re-suspending them in PBS due to the screening of the charges in a medium with high ionic strength.

The changes in hydrodynamic radius of SPIO-PNPs were investigated by DLS at room and body temperature over one month. The hydrodynamic radius did not change substantially during this period of time. This could be attributed to the repulsive force between negatively charged particles and the surfactant-like behavior of amphiphilic di-block

copolymer used as a matrix for encapsulation of SPIO-NPs.

The cytotoxicity of SPIO-PNPs in two different concentrations, SPIO-NPs and PNPs were studied over course of three days on MDA-MB-231 breast cancer cell line. The cell viability for all the above mentioned systems was high (over 85%) which means that that they did not induce toxicity.

The successful internalization of SPIO-PNPs was visualized by TEM. The cells were fixed and cross sectioned to make sure that the particles were inside the cell. TEM micrographs confirmed that the particles were successfully internalized and confined within vesicles via endocytosis mechanism.

Magnetic nanocarriers with an iron oxide core and a biodegradable and biocompatible polymer shell can greatly enhance the targetability of drug delivery systems. PSA-mPEG could be promising for magnetic drug delivery systems due to its biocompatibility and biodegradability. Besides PSA block can provide a sustained drug delivery system while the PEG block increases the circulation time in blood stream. These magnetic nanocarrier systems can be combined with other targeting systems like ligand targeting to form a more efficient drug delivery system.

References

1. Marcu, A., Pop, S., Dumitrache, F., Mocanu, M., Niculite, C.M., Gherghiceanu, M., Lungu, C.P., Fleaca, C., Ianchis, R., Barbut, A., Grigoriu, C. and Morjan, I., *Magnetic iron oxide nanoparticles as drug delivery system in breast cancer.* Applied Surface Science, 2013. **281**: p. 60-65.

2. Gao, W., Xiang, B., Meng, T.T., Liu, F. and Qi, X.R., *Chemotherapeutic drug delivery to cancer cells using a combination of folate targeting and tumor microenvironment-sensitive polypeptides.* Biomaterials, 2013. **34**(16): p. 4137-49.

3. Lu, R.M., Chen, M.S., Chang, D.K., Chiu, C.Y., Lin, W.C., Yan, S.L., Wang, Y.P., Kuo, Y.S., Yeh, C.Y., Lo, A. and Wu, H.C., *Targeted drug delivery systems mediated by a novel Peptide in breast cancer therapy and imaging.* PLoS One, 2013. **8**(6): p. e66128.

4. You, J.O., Guo, P. and Auguste, D.T., *A drug-delivery vehicle combining the targeting and thermal ablation of HER2+ breast-cancer cells with triggered drug release.* Angew Chem Int Ed Engl, 2013. **52**(15): p. 4141-6.

5. Panyam, J. and Labhasetwar, V., *Biodegradable nanoparticles for drug and gene delivery to cells and tissue.* Advanced Drug Delivery Reviews, 2012. **64**: p. 61-71.

6. Santhosh, P.B. and Ulrih, N.P., *Multifunctional superparamagnetic iron oxide nanoparticles: promising tools in cancer theranostics.* Cancer Lett, 2013. **336**(1): p. 8-17.

7. Letchford, K. and Burt, H., *A review of the formation and classification of amphiphilic block copolymer nanoparticulate structures: micelles, nanospheres, nanocapsules and polymersomes.* Eur J Pharm Biopharm, 2007. **65**(3): p. 259-69.

8. Ambikanandan, M., Kiruba, F., Manisha, L. and Tapan, S., *Surfactants and Block Copolymers in Drug Delivery*, in *Colloids in Drug Delivery*. 2010, CRC Press. p. 1-53.

9. Vauthier, C. and Bouchemal, K., *Methods for the preparation and manufacture of polymeric nanoparticles.* Pharm Res, 2009. **26**(5): p. 1025-58.

10. Fessi, H., Puisieux, F., Devissaguet, J.P., Ammoury, N. and Benita, S., *Nanocapsule formation by interfacial polymer deposition following solvent displacement.* International Journal of Pharmaceutics, 1989. **55**(1): p. R1-R4.

11. Discher, D.E. and Eisenberg, A., *Polymer vesicles.* Science, 2002. **297**(5583): p. 967-73.

12. Lammers, T., Hennink, W.E. and Storm, G., *Tumour-targeted nanomedicines: principles and practice.* Br J Cancer, 2008. **99**(3): p. 392-7.

13. Ruoslahti, E., Bhatia, S.N. and Sailor, M.J., *Targeting of drugs and nanoparticles to tumors.* J Cell Biol, 2010. **188**(6): p. 759-68.

14. Park, E.K., Kim, S.Y., Lee, S.B. and Lee, Y.M., *Folate-conjugated methoxy poly(ethylene glycol)/poly(epsilon-caprolactone) amphiphilic block copolymeric micelles for tumor-targeted drug delivery.* J Control Release, 2005. **109**(1-3): p. 158-68.

15. Doiron, A., Betancourt, T. and Brannon-Peppas, L., *Polymeric Nanoparticles for Tumor-Targeted Drug Delivery*, in *Nanotechnology for Cancer Therapy*. 2006, CRC Press. p. 215-229.

16. Bertrand, N., Wu, J., Xu, X., Kamaly, N. and Farokhzad, O.C., *Cancer nanotechnology: The impact of passive and active targeting in the era of modern cancer biology.* Adv Drug Deliv Rev, 2013.

17. Jain, R.K. and Stylianopoulos, T., *Delivering nanomedicine to solid tumors.* Nat Rev Clin Oncol, 2010. **7**(11): p. 653-64.

18. Swartz, M.A., *The physiology of the lymphatic system.* Advanced Drug Delivery Reviews, 2001. **50**(1–2): p. 3-20.

19. Mansoor, M.A., Dinesh, B.S. and Sushma, K., *Long-Circulating Polymeric Nanoparticles for Drug and Gene Delivery to Tumors*, in *Nanotechnology for Cancer Therapy*. 2006, CRC Press. p. 231-242.

20. Douziech-Eyrolles, L., Marchais, H., Herve, K., Munnier, E., Souce, M., Linassier, C., Dubois, P. and Chourpa, I., *Nanovectors for anticancer agents based on superparamagnetic iron oxide nanoparticles.* International Journal of Nanomedicine, 2007. **2**(4): p. 541-550.

21. Reimhult, E., *Imaging and Triggered Release through Design of Ultrastable Core-Shell Iron Oxide Nanoparticles*, in *Bioengineered Nanomaterials*. 2013, CRC Press. p. 177-198.

22. Dilnawaz, F., Singh, A., Mohanty, C. and Sahoo, S.K., *Dual drug loaded superparamagnetic iron oxide nanoparticles for targeted cancer therapy.* Biomaterials, 2010. **31**(13): p. 3694-706.

23. Mahmoudi, M., Sant, S., Wang, B., Laurent, S. and Sen, T., *Superparamagnetic iron oxide nanoparticles (SPIONs): development, surface modification and applications in chemotherapy.* Adv Drug Deliv Rev, 2011. **63**(1-2): p. 24-46.

24. Cole, A.J., Yang, V.C. and David, A.E., *Cancer theranostics: the rise of targeted magnetic nanoparticles.* Trends Biotechnol, 2011. **29**(7): p. 323-32.

25. Mody, V.V., Cox, A., Shah, S., Singh, A., Bevins, W. and Parihar, H., *Magnetic nanoparticle drug delivery systems for targeting tumor.* Applied Nanoscience, 2013.

26. Wadajkar, A.S., Menon, J.U., Tsai, Y.S., Gore, C., Dobin, T., Gandee, L., Kangasniemi, K., Takahashi, M., Manandhar, B., Ahn, J.M., Hsieh, J.T. and Nguyen, K.T., *Prostate cancer-specific thermo-responsive polymer-coated iron oxide nanoparticles.* Biomaterials, 2013. **34**(14): p. 3618-25.

27. Prashant, C., Dipak, M., Yang, C.T., Chuang, K.H., Jun, D. and Feng, S.S., *Superparamagnetic iron oxide--loaded poly(lactic acid)-D-alpha-tocopherol polyethylene glycol 1000 succinate copolymer nanoparticles as MRI contrast agent.* Biomaterials, 2010. **31**(21): p. 5588-97.

28. Dias, A.M., Hussain, A., Marcos, A.S. and Roque, A.C., *A biotechnological perspective on the application of iron oxide magnetic colloids modified with polysaccharides.* Biotechnol Adv, 2011. **29**(1): p. 142-55.

29. Gupta, A.K. and Gupta, M., *Synthesis and surface engineering of iron oxide nanoparticles for biomedical applications.* Biomaterials, 2005. **26**(18): p. 3995-4021.

30. Thorek, D.L., Chen, A.K., Czupryna, J. and Tsourkas, A., *Superparamagnetic iron oxide nanoparticle probes for molecular imaging.* Ann Biomed Eng, 2006. **34**(1): p. 23-38.

31. Pillai, V., Kumar, P., Hou, M.J., Ayyub, P. and Shah, D.O., *Preparation of nanoparticles of silver halides, superconductors and magnetic materials using water-in-oil microemulsions as nano-reactors.* Advances in Colloid and Interface Science, 1995. **55**(0): p. 241-269.

32. Supaphol, P., Suwantong, O., Sangsanoh, P., Srinivasan, S., Jayakumar, R. and Nair, S.V., *Electrospinning of Biocompatible Polymers and Their Potentials in Biomedical Applications.* 2011. **246**: p. 213-239.

33. Nair, L.S. and Laurencin, C.T., *Biodegradable polymers as biomaterials.* Progress in Polymer Science, 2007. **32**(8-9): p. 762-798.

34. De Souza, R., Zahedi, P., Allen, C.J. and Piquette-Miller, M., *Polymeric drug delivery systems for localized cancer chemotherapy.* Drug Deliv, 2010. **17**(6): p. 365-75.

35. Attenello, F.J., Mukherjee, D., Datoo, G., McGirt, M.J., Bohan, E., Weingart, J.D., Olivi, A., Quinones-Hinojosa, A. and Brem, H., *Use of Gliadel (BCNU) wafer in the surgical treatment of malignant glioma: a 10-year institutional experience.* Ann Surg Oncol, 2008. **15**(10): p. 2887-93.

36. Elstad, N.L. and Fowers, K.D., *OncoGel (ReGel/paclitaxel)--clinical applications for a novel paclitaxel delivery system.* Adv Drug Deliv Rev, 2009. **61**(10): p. 785-94.

37. Kumar, N., Langer, R.S. and Domb, A.J., *Polyanhydrides: an overview.* Advanced Drug Delivery Reviews, 2002. **54**(7): p. 889-910.

38. Katti, D.S., Lakshmi, S., Langer, R. and Laurencin, C.T., *Toxicity, biodegradation and elimination of polyanhydrides.* Advanced Drug Delivery Reviews, 2002. **54**(7): p. 933-961.

39. Gomez-Lopera, S.A., Plaza, R.C. and Delgado, A.V., *Synthesis and Characterization of Spherical Magnetite/Biodegradable Polymer Composite Particles.* J Colloid Interface Sci, 2001. **240**(1): p. 40-47.

40. Schleich, N., Sibret, P., Danhier, P., Ucakar, B., Laurent, S., Muller, R.N., Jerome, C., Gallez, B., Preat, V. and Danhier, F., *Dual anticancer drug/superparamagnetic iron oxide-loaded PLGA-based nanoparticles for cancer therapy and magnetic resonance imaging.* Int J Pharm, 2013. **447**(1-2): p. 94-101.

41. Filippousi, M., Altantzis, T., Stefanou, G., Betsiou, M., Bikiaris, D.N., Angelakeris, M., Pavlidou, E., Zamboulis, D. and Van Tendeloo, G., *Polyhedral iron oxide core–shell nanoparticles in a biodegradable polymeric matrix: preparation, characterization and application in magnetic particle hyperthermia and drug delivery.* RSC Advances, 2013. **3**(46): p. 24367.

42. Chan, C.-K. and Chu, I.M., *Crystalline and dynamic mechanical behaviors of synthesized poly(sebacic anhydride-co-ethylene glycol).* Biomaterials, 2003. **24**(1): p. 47-54.

43. Clogston, J.D. and Patri, A.K., *Zeta potential measurement.* Methods Mol Biol, 2011. **697**: p. 63-70.

44. Anja, G., Karen, K.-G.I. and Thomas, R., *Poly(Alkyl Cyanoacrylate) Nanoparticles for Drug Delivery and Vaccine Development*, in *Colloids in Drug Delivery*. 2010, CRC Press. p. 99-135.

45. Jatin, K., Somnath, S. and Alekha, K.D., *Multiple Emulsions*, in *Colloids in Drug Delivery*. 2010, CRC Press. p. 177-202.

46. Kjoniksen, A.L., Zhu, K., Behrens, M.A., Pedersen, J.S. and Nystrom, B., *Effects of temperature and salt concentration on the structural and dynamical features in aqueous solutions of charged triblock copolymers.* J Phys Chem B, 2011. **115**(10): p. 2125-39.

47. Liang, Y., Xiao, L., Zhai, Y., Xie, C., Deng, L. and Dong, A., *Preparation and characterization of biodegradable poly(sebacic anhydride) chain extended by glycol as drug carrier.* Journal of Applied Polymer Science, 2013. **127**(5): p. 3948-3953.

48. Zhang, N. and Guo, S.-R., *Synthesis and micellization of amphiphilic poly(sebacic anhydride)-poly(ethylene glycol)-poly(sebacic anhydride) block copolymers.* Journal of Polymer Science Part A: Polymer Chemistry, 2006. **44**(3): p. 1271-1278.

49. Ellis, E.A., *Correlative transmission microscopy: cytochemical localization and immunocytochemical localization in studies of oxidative and nitrosative stress.* Methods Mol Biol, 2008. **477**: p. 41-8.

50. Okassa, L.N., Marchais, H., Douziech-Eyrolles, L., Herve, K., Cohen-Jonathan, S., Munnier, E., Souce, M., Linassier, C., Dubois, P. and Chourpa, I., *Optimization of iron oxide nanoparticles encapsulation within poly(d,l-lactide-co-glycolide) sub-micron particles.* Eur J Pharm Biopharm, 2007. **67**(1): p. 31-8.

51. Louis, K.S. and Siegel, A.C., *Cell viability analysis using trypan blue: manual and automated methods.* Methods Mol Biol, 2011. **740**: p. 7-12.

52. Chan, C.-K. and Chu, I.M., *In vitro release of incorporated model compounds in poly(sebacic anhydride-co-ethylene glycol).* European Polymer Journal, 2005. **41**(6): p. 1403-1409.

53. Chan, C.-K. and Chu, I.M., *In vitro degradation of poly(sebacic anhydride-co-ethylene glycol).* Materials Chemistry and Physics, 2004. **88**(1): p. 59-66.

54. Lim, H.J., Nam, H.Y., Lee, B.H., Kim, D.J., Ko, J.Y. and Park, J.-s., *A Novel Technique for Loading of Paclitaxel-PLGA Nanoparticles onto ePTFE Vascular Grafts.* Biotechnology Progress, 2007. **23**(3): p. 693-697.

55. Cho, K., Wang, X., Nie, S., Chen, Z.G. and Shin, D.M., *Therapeutic nanoparticles for drug delivery in cancer.* Clin Cancer Res, 2008. **14**(5): p. 1310-6.

56. Na, K., Bum Lee, T., Park, K.-H., Shin, E.-K., Lee, Y.-B. and Choi, H.-K., *Self-assembled nanoparticles of hydrophobically-modified polysaccharide bearing vitamin H as a targeted anti-cancer drug delivery system.* European Journal of Pharmaceutical Sciences, 2003. **18**(2): p. 165-173.

57. Acharya, S. and Sahoo, S.K., *PLGA nanoparticles containing various anticancer agents and tumour delivery by EPR effect.* Adv Drug Deliv Rev, 2011. **63**(3): p. 170-83.

58. Kjøniksen, A.-L., Hiorth, M. and Nyström, B., *Association under shear flow in aqueous solutions of pectin.* European Polymer Journal, 2005. **41**(4): p. 761-770.

59. P. Sommerfeld, B.A.S., U. Schroeder, *Long-term stability of PBCA nanoparticle suspensions.* Journal of Microencapsulation, 2000. **17**(1): p. 69-79.

60. Jeong, Y.-I., Cho, C.-S., Kim, S.-H., Ko, K.-S., Kim, S.-I., Shim, Y.-H. and Nah, J.-W., *Preparation of poly(DL-lactide-co-glycolide) nanoparticles without surfactant.* Journal of Applied Polymer Science, 2001. **80**(12): p. 2228-2236.

61. Al-Manasir, N., Zhu, K., Kjoniksen, A.L., Knudsen, K.D., Karlsson, G. and Nystrom, B., *Effects of temperature and pH on the contraction and aggregation of microgels in aqueous suspensions.* J Phys Chem B, 2009. **113**(32): p. 11115-23.

62. Ge, X., Jackson, R.L., Liu, J., Harper, E.A., Hoffer, M.E., Wassel, R.A., Dormer, K.J., Kopke, R.D. and Balough, B.J., *Distribution of PLGA nanoparticles in chinchilla cochleae.* Otolaryngol Head Neck Surg, 2007. **137**(4): p. 619-23.

63. Sonvico, F., Mornet, S., Vasseur, S., Dubernet, C., Jaillard, D., Degrouard, J., Hoebeke, J., Duguet, E., Colombo, P. and Couvreur, P., *Folate-Conjugated Iron Oxide Nanoparticles for Solid Tumor Targeting as Potential Specific Magnetic Hyperthermia Mediators: Synthesis, Physicochemical Characterization, and in Vitro Experiments.* Bioconjugate Chemistry, 2005. **16**(5): p. 1181-1188.

64. Ankamwar, B., Lai, T.C., Huang, J.H., Liu, R.S., Hsiao, M., Chen, C.H. and Hwu, Y.K., *Biocompatibility of Fe(3)O(4) nanoparticles evaluated by in vitro cytotoxicity assays using normal, glia and breast cancer cells.* Nanotechnology, 2010. **21**(7): p. 75102.

65. Singh, N., Jenkins, G.J., Asadi, R. and Doak, S.H., *Potential toxicity of superparamagnetic iron oxide nanoparticles (SPION).* Nano Rev, 2010. **1**.

66. Zhao, A., Zhou, S., Zhou, Q. and Chen, T., *Thermosensitive micelles from PEG-based ether-anhydride triblock copolymers.* Pharm Res, 2010. **27**(8): p. 1627-43.

67. Mukherjee, S., Ghosh, R.N. and Maxfield, F.R., *Endocytosis.* Physiol Rev, 1997. **77**(3): p. 759-803.

68. Wilhelm, C., Billotey, C., Roger, J., Pons, J.N., Bacri, J.C. and Gazeau, F., *Intracellular uptake of anionic superparamagnetic nanoparticles as a function of their surface coating.* Biomaterials, 2003. **24**(6): p. 1001-1011.